Numerical study of thermomechanical behaviour of reinforced concrete beams with and without textile reinforced concrete (TRC) strengthening: Effects of TRC thickness and thermal loading rate

Najib Douk, Xuan Hong Vu, Amir Si Larbi, Maxime Audebert, Robin Chatelin

Numerical study of thermomechanical behaviour of reinforced concrete beams with and without textile reinforced concrete (TRC) strengthening: effects of TRC thickness and thermal loading rate

Najib Douk[1a], Xuan Hong Vu[*2], Amir Si Larbi[1b], Maxime Audebert[1c] and Robin Chatelin[1d]

[1]*University of Lyon, ENISE, LTDS (UMR 5513 CNRS), 58 rue Jean Parot, 42023 Saint-Etienne, France.*
[2]*Université de LYON, Univérsité Claude Bernard LYON 1; Laboratoire des Matériaux Composites pour la Construction LMC2, Lyon, France.*

(Received keep as blank , revised keep as blank , Accepted keep as blank)

Abstract.
This study analyses the thermomechanical behaviour of steel-reinforced concrete (RC) beams strengthened with textile reinforced concrete (TRC) under mechanical and fire loads (i.e., the standard fire curve, ISO-834). Two main aspects are investigated. First, the effect of the TRC's thickness on the thermomechanical behaviour of RC beams is assessed. Then, the thermomechanical behaviour of RC beams strengthened with TRC is numerically modelled for different heating rates (i.e., heating scenarios). The results and conclusions of this study clarify the thermomechanical contributions of TRC to RC structural elements subjected to fire scenarios.

Keywords: Textile reinforced concrete (TRC); fire scenarios; ISO-834; numerical modelling; reinforced concrete beams.

1. Introduction

After the tragic incidents that occurred in the Mont Blanc tunnel in 1999 and the Eurotunnel in 1996, many researchers began studying the behaviour of concrete in fire scenarios. When a slab of concrete is exposed to fire, its thermal and mechanical properties degenerate as a result of the various physicochemical changes that occur. Several authors have studied the behaviour of fibre reinforced concretes (FRCs) at elevated temperatures [1] for steel, basalt, and hybrid FRCs; and [2] steel fibre reinforced self-compacting concrete. These studies established the evolution of the residual compressive strength of FRC after exposure to a fire and different elevated temperature levels. Other phenomena, such as the thermal and hydric gradients that induce spalling in heated high-performance concretes, have been reported in some studies [3]. If reinforced concrete (RC) elements are exposed to fire long enough, they become unable to continue supporting the mechanical loads they were initially designed to sustain. Carbon fibre reinforced polymer (CFRP) was used for decades to reinforce concrete structures to improve their mechanical strength. A study [4] showed that CFRP reinforced concrete subjected to fire is sufficiently strong in the first few minutes of fire exposure (according to standard fire curve ISO-834). Failure occurs once the CFRP and CFRP/concrete interface temperature exceeds 200 °C, which is the critical temperature of the paste used to bond the CFRP to the concrete surface. Beyond this critical temperature, the CFRP/concrete bond shear resistance is reduced to zero, which results in the reinforced structural element behaving like a non-reinforced one. Furthermore, at high temperatures, CFRP releases toxic fumes which are hazardous to the residents of buildings that have experienced fires. To mitigate this hazard, a novel method of strengthening structural elements with a new material, a textile reinforced concrete (TRC), at elevated temperatures (i.e., fire exposure) is analysed and discussed in this study.

TRC, TRM (textile reinforced mortar), and FRCM (fibre reinforced cementitious matrix) are part of a new generation of composite materials. These materials draw their mechanical advantages from textile reinforcement

[*]Corresponding author, Associate professor, Ph.D., E-mail: Xuan-Hong.Vu@univ-lyon1.fr
[a] Ph.D., E-mail: najib.douk@gmail.com
[b] Professor, Ph.D., E-mail: amir.si-larbi@enise.fr
[c] Associate Professor, Ph.D., E-mail: maxime.audebert@enise.fr
[d] Associate Professor, Ph.D., E-mail: robin.chatelin@enise.fr

grids (like FRP), but they have a mineral matrix that enhances their fire stability at high temperatures compared to their traditional counterpart (CFRP).

TRCs have a good mechanical performance at ambient temperatures; however, few studies have evaluated, either experimentally or numerically, their behaviour at high temperatures. Even fewer studies have addressed the suitability of TRCs within the context of structural rehabilitation.

In this context, two crucial aspects of structural stability under fire conditions were addressed in this study:

- A numerical study was performed on the thermomechanical behaviour of RC beams (reference beams and TRC strengthened beams) and the effect of the TRC thickness on the local and global scales.
- A numerical study was performed on the thermomechanical behaviour of TRC strengthened RC beams and the effect of the heating rate on the local and global mechanical reactions.

The mechanical behaviour of RC concrete beams strengthened with TRC at room temperature has been studied by many authors ([5], [6], [7], [8], [9], [10], [11], [12], [13], [14], and [15]). These studies have highlighted the contribution of TRCs to the mechanical strength of TRC-reinforced beams under simple bending loads. A TRC is a composite material made of a cementitious matrix reinforced with textiles [16], [17], [18], and [15]. The potential for TRC to be used as a strengthening component in RC beams under fire conditions comes from its bonding system, as these composites are attached to structural surfaces with cementitious pastes. These pastes, unlike the polymer pastes used for CFRP composites, are more likely to retain their mechanical properties for a longer period of time under fire conditions.

In the experimental literature, at the structural scale, various studies have detailed the fire behaviour of RC beams strengthened with cementitious matrix-based composites. Ehlig et al. [19] evaluated carbon fibre-reinforced fine-grained concrete, and Bisby [20] and Bisby et al. [21] evaluated structural elements reinforced with TRM and FRCM up to 500 °C. More work was done by Michels et al. [22], Maroudas et al. [23], Tetta et al. [8], and Raoof et al. [24] on FRCM and TRC at elevated temperatures. These studies showed that the TRC-strengthened specimens maintained an average of 85% of their initial bond strength up to 400 °C, and, overall, the TRC exhibited good performance at elevated temperatures.

At the material scale, few studies on the behaviour of TRC under fire loads have been performed ([25], [26], [27], and [28]) at temperatures ranging from 20 °C to 400 °C. Some exhaustive studies on the thermomechanical behaviour of TRC and its link to the constitutive materials were carried out by Nguyen et al. [18] and Tlaiji et al. [16], although no structural fire tests were performed.

In the numerical literature on composite reinforced structural elements, few have evaluated TRC [29]. However, when TRCs are addressed, it is always with a focus on the material scale. In contrast, CFRP strengthened RC has been widely studied by many authors, and these studies have covered almost every scale and aspect of that strengthening procedure. Firmo et al. ([30], [31]) and Hawileh et al. ([32], [33]) carried out different studies on CFRP strengthened RC beams under fire loads, and these studies commonly reported that the efficiency of CFRP is quickly reduced in the event of a fire. In recent years, several researchers ([34], [35]) have participated in advancing the numerical tools used to predict the thermomechanical behaviour of CFRP strengthened structural elements.

A recent critical study [36] on CFRP strengthened RC beams summarised the findings of several studies on this matter. This study pointed that the weakness of CFRP in high temperature environments can be overcome by the incorporation of fire protection systems.

The response of RC beams in different fire scenarios is one of the interesting aspects of structural behaviour in fire scenarios. Some authors have numerically [37] and experimentally [38] assessed this aspect for unstrengthened RC beams in which the temperatures and deflections were measured over time. These studies commonly reported that the higher the heating rate was, the faster the temperature increased in the concrete element. Therefore, two important findings were noted. First, higher heating rates caused higher deflection rates. Second, it was observed that specimen failure occurred sooner with higher heating rates.

To the best of the authors' knowledge, there is no numerical or experimental study that addresses the contribution of TRC to the thermomechanical behaviour of RC beams in a fire scenario (ISO-834). The effects of the TRC thickness and thermal loading rate on the global and local behaviour of steel-reinforced concrete beams (with or without TRC strengthening) have not yet been studied.

In this study, as a first step, two numerical models of a reference RC beam in a fire scenario (i.e., without TRC strengthening) were built and validated by comparing the numerical results with experimental results (e.g., mid-span deflections and axial strains and stresses in the concrete coating, steel rebar, and TRC). This purpose of this step was to confirm the reliability of the RC thermomechanical elasto-plastic model. Once the numerical-experimental comparison was validated, a numerical model of an RC beam strengthened with TRC was built based on the validated thermomechanical models and the experimental results of fire tests carried out on a TRC.

This numerical model of an RC beam strengthened with TRC was used to carry out the parametric studies mentioned above on a structural scale.

In the following sections, the numerical approach, thermal actions, and thermo-physical properties of the constitutive materials are presented. Thereafter, the results of the numerical models are discussed. Lastly, the main conclusions are presented.

2. Test specimens used to validate the numerical thermomechanical model

For the numerical validation, two experimental studies on structural elements under fire conditions were selected (i.e., [39] and [40]). Two reasons guided the selection of these particular studies. First, they provided a complete set of information about the tests performed. Second, they took into consideration the load application order, which allowed the real life fire scenario to be recreated (i.e., a mechanical load, then a thermal load). In addition, the specimens were of a structural size as opposed to the oven sized beams that are usually encountered in these types of studies.

In experimental environments, the mechanical load is delivered by applying a displacement piloted piston to the surface of the RC beam until a certain mechanical load (i.e., service load) is reached; then, the thermal load (according to standard fire curve, ISO-834, shown in Fig. 1) is applied to the surfaces of the beam. The service mechanical load is maintained at a constant value during thermal loading in order to achieve a condition as close to the reality of a fired building as possible.

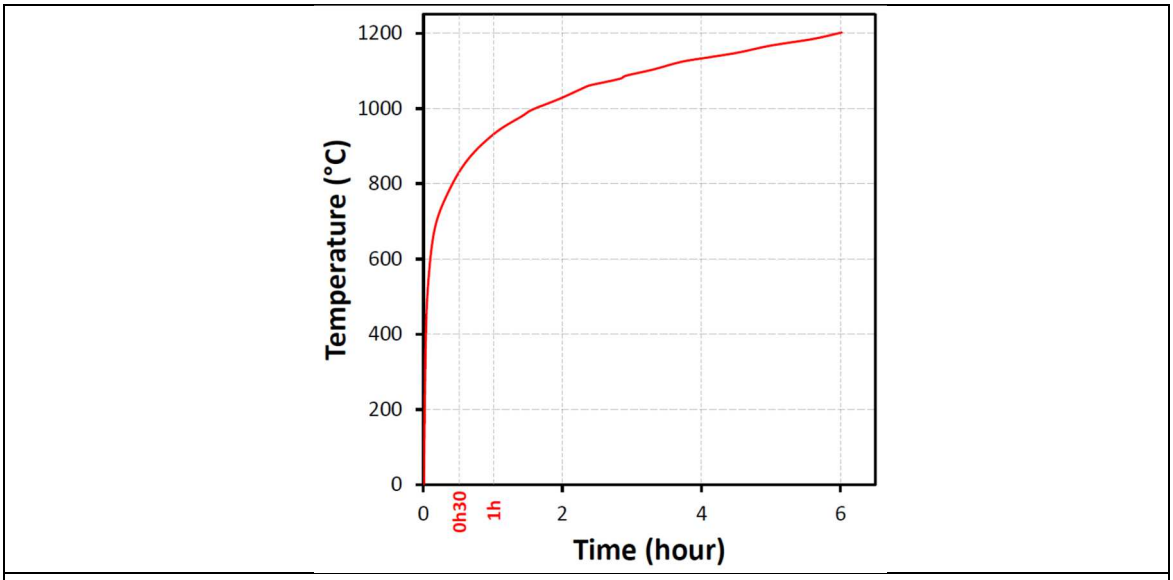

Fig. 1. Temperature evolution with time of the ISO-834 curve

Table 1 and Fig. 2-3 summarize the necessary information of the chosen experimental test specimens. At first, a mechanical load was applied to the specimens. Once the mechanical loads were fully applied, the beams already installed in the test ovens were exposed to air heating up at an ISO-834 rate.

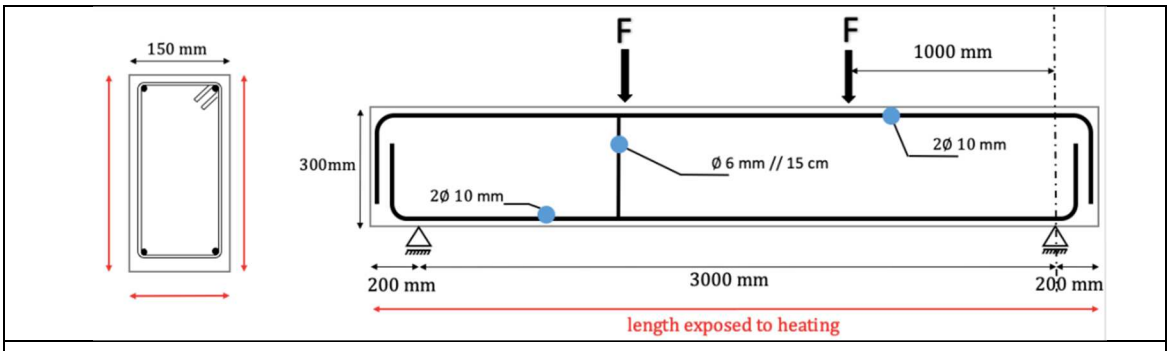

Fig. 2. Geometry of "Test Specimen 1" [39]

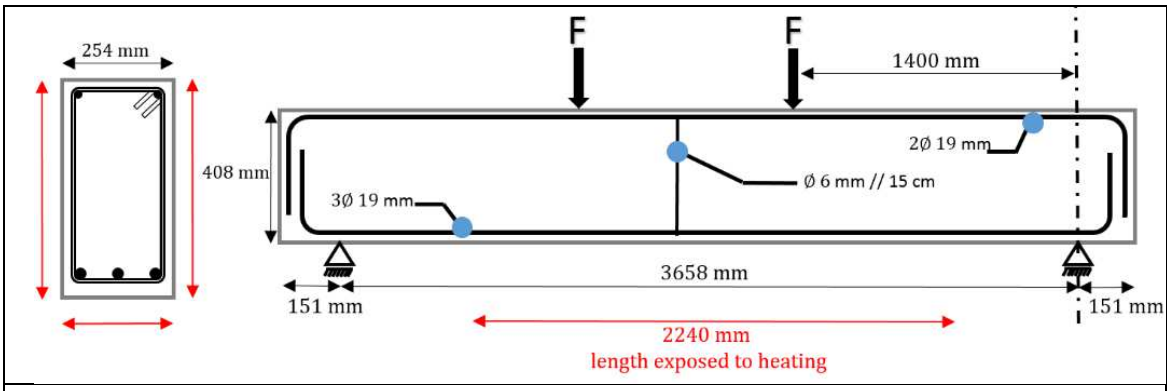

Fig. 3. Geometry of "Test Specimen 2" [40]

Table 1 Specific information about the experimental test specimens [experimental data sources: [39], [40]

	Test Specimen 1 [39]	Test specimen 2 [40]
Concrete strength (MPa) (mean value)	30, 1	32
Steel strength (MPa)	500	542
Thermal load	ISO-834 (lateral and bottom surfaces) see Fig. 2	ISO-834 (lateral and bottom surfaces) see Fig. 3
Mechanical load	24 kN (4-point bending test) see Fig. 2	50 kN each force (4-point bending test) see Fig. 3

3. Numerical methods

The finite element method (FEM) was used in the MSC Software MARC MENTAT software [41]. This section focuses on the numerical approach where the thermal and thermomechanical hypotheses are established. Then, the test specimens are presented, and, finally, the numerical models are introduced.

3.1. Numerical approach

The numerical implementation of the thermal aspects of concrete is quite complex. A quick state-of-the-art review revealed two different approaches. The thermo-hydro-mechanical (THM) method is a complex approach [42] that considers concrete to be a three phase-entity comprised of solid concrete, liquid, and gas. However, the most popular approach for structural element analysis is the thermomechanical method, which considers concrete to be a homogenous entity. In the latter approach, the thermal calculations are incorporated into the mechanical analysis through the material properties degradation and thermal dilatation. It must be stated that the mechanical part is not taken into consideration in the thermal calculations (i.e., weak thermomechanical coupling). This assumption is supported by the fact that very small thermal transfers occur as a result of the mechanical motion of the RC.

Since this numerical work was carried out at the structural scale, the THM approach was determined to be too refined for this scale. Therefore, the thermomechanical approach was used in this study.

In the following sections, the fire tests on the RC beams, which are used as the basis of the validation of the numerical model, are presented. Then, the main hypotheses of the thermomechanical model of the RC beams (with or without a TRC) are introduced. Finally, a numerical-experimental validation is carried out, and the numerical results are presented and discussed.

3.2. Thermal actions, thermal properties of the materials, and input data for the models

The thermal action implemented in the numerical simulations of the heating process is the same action used during fire resistance tests, namely the ISO-834 nominal thermal action, which is defined by Eq. (1).

$$\theta_g = \theta_0 + 345 \log(8t+1) \quad (1)$$

where θ_g is the gas temperature of the oven in degrees Celsius (°C), θ_0 is the initial temperature (°C), and t is the time of fire exposure (min).

The heat quantity received by the concrete element under thermal action at time t, is defined by the sum of the convective and radiative flows. $\varepsilon = 0.7$ is the emissivity of the steel [43], and $\varepsilon = 0.9$ is the emissivity of the concrete [44] (see Eq. (2)).

The three classical heat transfer modes were taken into account: radiation (see Eq. (2)), convection (see Eq. (3)) at the surfaces exposed to the thermal flux, and conduction (see Eq. (4)) within the constitutive materials. Once the thermal calculations were completed, a map of the temperature fields of the specimen was extracted from the calculations for every increment. This map was implemented later on in the mechanical analysis as a thermal boundary condition. The thermal dilation and degradation of the steel's and concrete's mechanical properties [44] were then calculated following the thermal map calculated earlier. It should be noted that, during the thermal calculations, the thermal dilation was not taken into consideration. The thermal radiation and convection could not be calculated in the MARC MENTAT software's basic interface for a phenomenon as complex as a fire. Consequently, a subroutine (a program developed in FORTRAN) was integrated into the thermal analysis to consider those thermal transfer modes.

- Thermal radiation

$$\Phi_r = \varepsilon \cdot \sigma \left(T_\infty^4 - T^4\right) \tag{2}$$

ε: Emissivity (less than 1) (dimensionless)
σ: Stefan's constant: 5.67×10^{-8} (W/ ($m^2 \cdot K^4$))

- Thermal convection

$$\Phi_c = h \cdot (T_f - T) \tag{3}$$

h: Thermal exchange coefficient
T_f: Fluid temperature (air temperature)
T: Solid temperature (structural element's surface)

- Thermal conduction

$$\varphi = -\lambda grad T \tag{4}$$

λ: Thermal conductivity
T: temperature

This numerical study was done in two steps. The first step was the thermal study. Once completed, as was stated earlier, the temperature fields were incorporated into the mechanical study. To carry out the numerical study through these two steps, the meshing had to be the same for both studies in order to incorporate the thermal fields into the mechanical analysis. Therefore, special attention was given to the meshing. During a previous study performed by the authors [45], the sensitivity of the thermal fields generated by the ISO-834 curve rate was assessed for different mesh sizes. It was found that a meshing size less than 4 cm delivered precise temperature fields in the case of an ISO-834 heating load. Therefore, rectangular shaped meshes with sides less than 4 cm were selected for the thermal and thermomechanical models in order to achieve high precision (see Section 3, "Numerical model results"). Hexagonal volumetric elements with eight integration points (i.e., Hex8) were used in the three-dimensional numerical models.

3.2.1. Concrete and TRC

Concrete is a very complex material, and its thermal characteristics vary with the evolution of its temperature. Therefore, in order to consider this intrinsic non-linearity, the thermal conductivity of concrete and the specific heat values implemented in the numerical model were set equal to the values recommended by Eurocode 2 (see Figs. 4a and 4b). It should be noted that Eurocode 2 established three curves of thermal conductivity, for concretes with siliceous, limestone and light aggregates (see Fig. 4a). However, the siliceous and limestone median curve was extracted and implemented in the thermal model. Regarding the specific heat, the upper curve of Fig. 4b, which shows the free interstitial water evaporation peak, was implemented in the thermal model.

As this is a thermomechanical study, and to take into consideration the effect of temperature on the overall mechanical and structural behaviour:

- The concrete's volumetric mass evolution with respect to temperature (Eurocode 2) was also implemented in the model. The implemented curve followed the relative evolution shown in Fig. 4c with an initial value of 2500 Kg/m^3 at 20 °C.
- Curve 1 and 2 from the Eurocode figure (Fig. 4d) show the thermal dilation of the siliceous and limestone aggregate-based concretes, respectively. A median curve of curves 1 and 2 was implemented in the model.

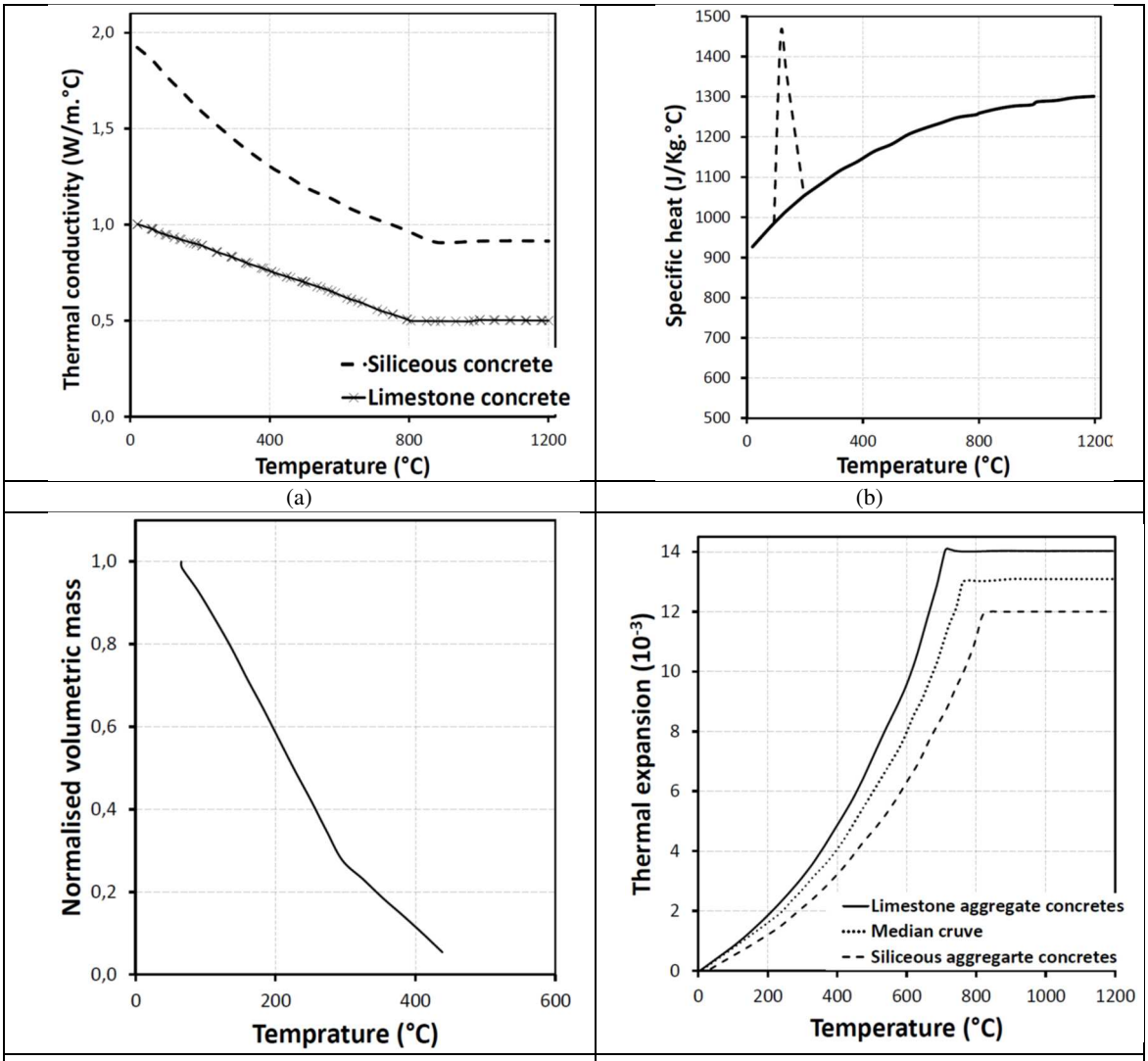

Fig. 4. Evolution of the thermal proprieties of concrete and/or TRC as a function of the temperature: (a) Thermal conductivity used for both the concrete and TRC (median curve was implemented) [44]; (b) Specific heat used for both the concrete and TRC (upper curve was implemented) [44]; (c) Volumetric mass used for both the concrete and TRC [46]; and (d) Thermal dilation used for only the concrete (median curve was implemented) [44]

The last parameter is the thermal expansion of the TRC. Tlaiji et al. [60] showed that the latter parameter is the result of complex microstructural events. On one hand, the TRC's cementitious matrix experiences shrinking at high temperatures. On the other hand, the textile's thermal expansion depends on the material's nature. As the thermal expansion coefficient of the TRC used for this numerical study (RCM100) was not experimentally characterised, the authors opted for the most conservative alternative, which is a null thermal expansion of the TRC model.

The effect of mechanical damage of concrete on its thermal conductivity and thermal behaviour of was not explicitly considered in this study. This allowed to note that with the level of mechanical loading applied to the steel-concrete beams studied in this study, the model developed made it possible to approximate the thermomechanical behavior of the beams.

3.2.2. Steel

Similar to concrete, the thermal properties of steel (Fig. 5a-b), and their evolution with respect to temperature, were incorporated into the thermal model. The thermal dilation (Fig. 5c) was also implemented in the thermomechanical model.

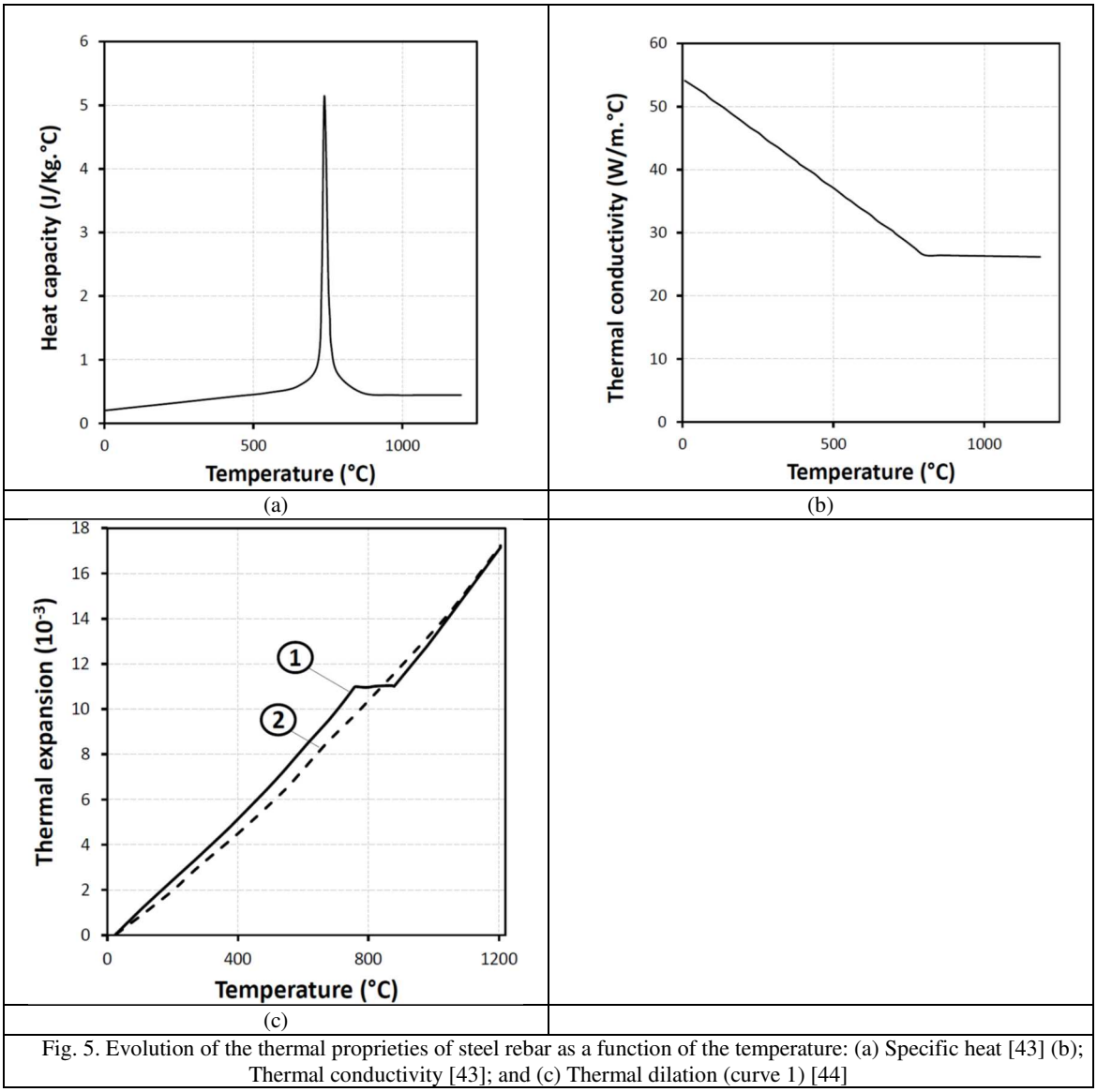

Fig. 5. Evolution of the thermal proprieties of steel rebar as a function of the temperature: (a) Specific heat [43] (b); Thermal conductivity [43]; and (c) Thermal dilation (curve 1) [44]

3.3. Thermomechanical properties of materials and input data for models

As shown in Fig. 6, the models specified in EN1992-1-2 [44] were adopted to identify the uniaxial properties of concrete at different elevated temperatures [47].

Insofar as this is essentially a uniaxial behaviour, the only mobilisation of the unidirectional behaviour of the constituent materials is sufficient to conduct numerical simulations.

3.3.1. Concrete and steel

An exhaustive literature review showed that the complexity of concrete's mechanical behaviour manifests in the difference in its behaviour in compression and tension, the non-linearity of the post-elastic behaviour, the non-linear dependence on the multi-dimensional state of stress, and the dependence of all these parameters on the temperature. Figures 6a–6c show the evolution of the uniaxial mechanical behaviour of concrete with respect

to the temperature. The relative evolution of the Young's modulus of concrete was extracted from the linear (i.e., elastic) part of Fig. 6b (compression). It should be noted that the normalised mechanical property (e.g., stress or Young's modulus) of a material is defined as the ratio between the value of the mechanical property at a specific temperature, T, and that at room temperature.

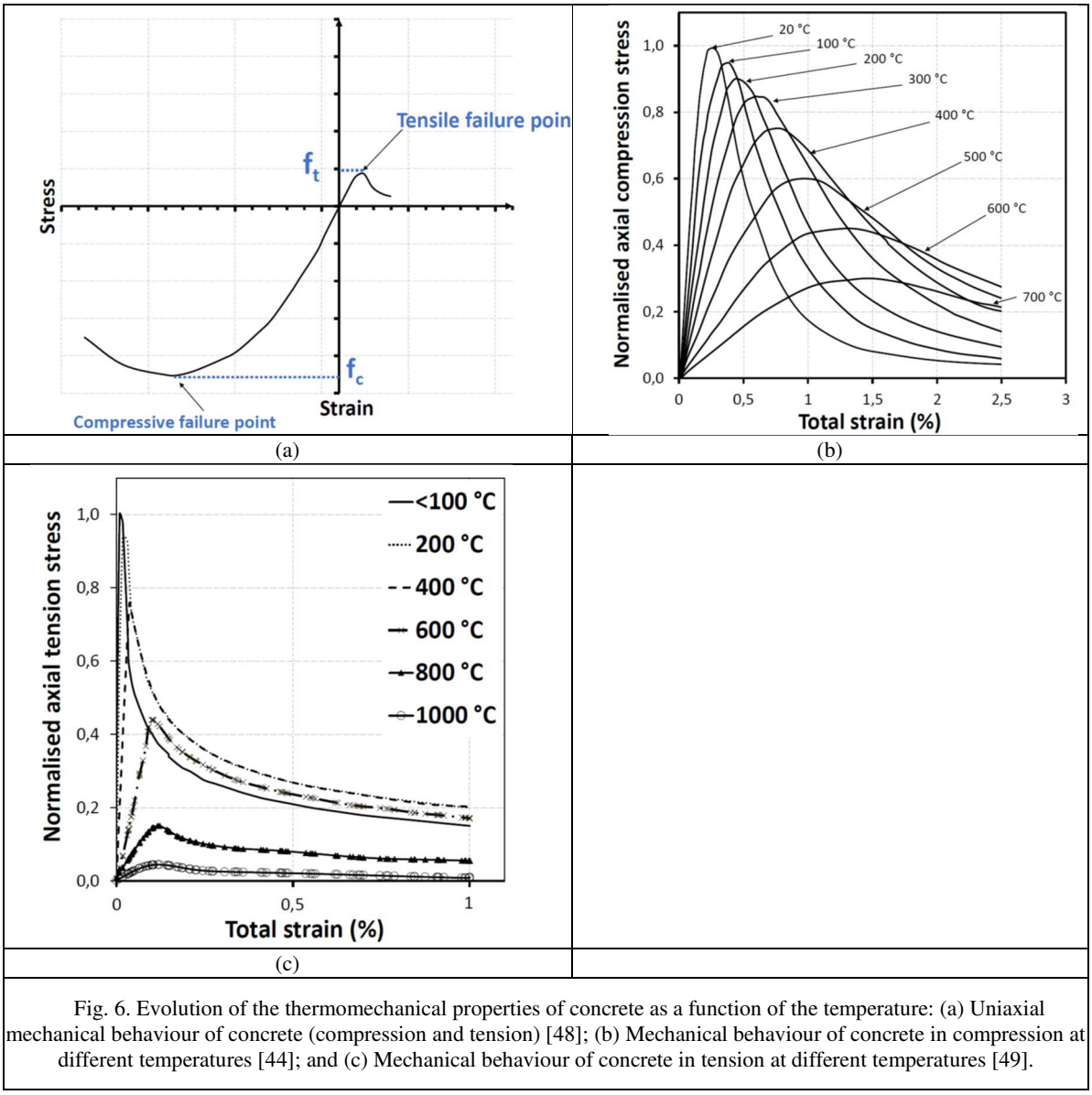

Fig. 6. Evolution of the thermomechanical properties of concrete as a function of the temperature: (a) Uniaxial mechanical behaviour of concrete (compression and tension) [48]; (b) Mechanical behaviour of concrete in compression at different temperatures [44]; and (c) Mechanical behaviour of concrete in tension at different temperatures [49].

Similar to concrete, the mechanical behaviour of steel at different temperatures was extracted from Eurocode 2 (Fig. 7a-7b) and incorporated in the thermomechanical model.

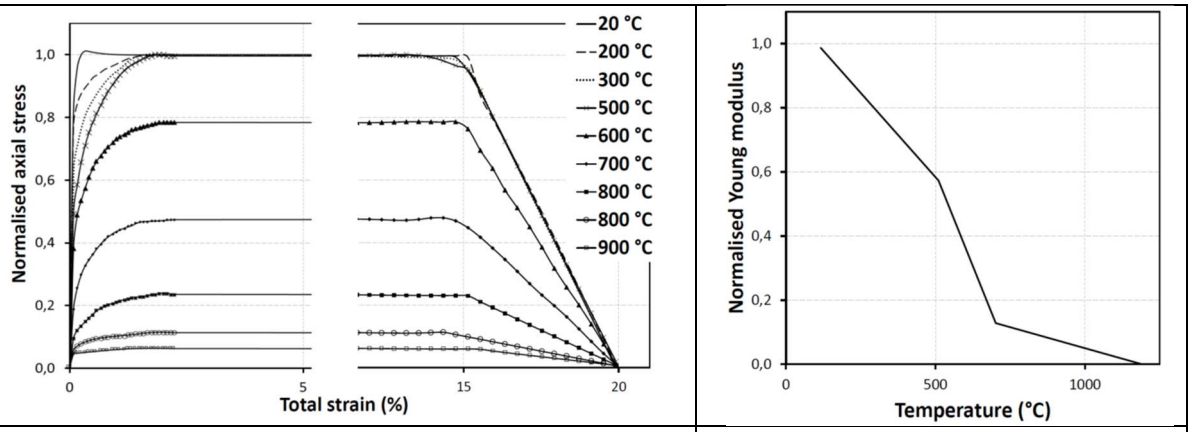

(a) (b)

Fig. 7. Evolution of the normalised mechanical properties of steel as a function of the temperature: (a) Mechanical behaviour of steel (similar in compression and tension) at different temperatures [44]; and (b) Evolution of the normalised Young's modulus of steel as function of the temperature [44]

3.3.2. Textile reinforced concrete (TRC)

Fig. 8a shows the mechanical behaviour of a TRC composite for four different temperatures (25 °C to 600 °C). Tlaiji et al. [50] experimentally assessed these curves. This experimental finding shows stress-strain curves of the TRC used as a strengthening material for RC beams. The tested TRC is composed of an aluminous matrix, 2 layers of chopped strand mat glass fibres and 2 layers of carbon grids, its reinforcement rate according to the traction direction is of 1.8% ($V_{f2} = V_{\text{carbon textile in tensile direction}}/V_{TRC}$). The elevated temperature tests consisted of getting TRC plates on constant temperatures (25 °C, 200 °C, 400 °C, and 600 °C) then tensile forces were applied on the tested specimens until failure, with a mechanical loading rate of 1 mm/min [50]. The numerical implementation procedure is explained in section 3.4.3. These thermomechanical tests were carried out according to a previously established protocol making it possible to characterise the behaviour of the TRC material at different temperatures independently with the experimental test conditions [18], [8]. In addition, the meshes of two carbon grids placed within studied TRC have the dimensions of 6 mm × 6 mm. There are approximately 8 meshes along the direction of the width of TRC tested (50 mm). Some control thermomechanical tests carried out on two TRC specimen sizes (50 mm and 100 mm) gave similar results. This result made it possible to confirm that the results of tests carried out on TRC specimens having width of 50 mm (due to the thermomechanical equipment used) can be applied for the behaviour of TRC in case of reinforcement of a reinforced concrete beam. It should be noted that these experimental findings were in good agreement with the general thermomechanical behaviour observed in previous experimental studies for textile-reinforced mortars under thermomechanical loads [51] and [18].

The fibers of the transverse direction are not used in the case of the present study. Textiles with bidirectional grids are often proposed for the strengthening of slabs and walls. Nevertheless, TRCs with grid textiles are also used to strengthen reinforced concrete beams (as in this case study). The transverse yarns do not directly take the tensile stresses in the longitudinal direction of the beams but they provide a great ease of laying of the TRC in the fresh state. Also, in case of accidental stresses, they allow the reinforced element a higher mechanical and thermal resistance in its transverse axis. Taking into account the elements mentioned above, textiles with bidirectional mechanical capabilities have been chosen for experimental thermomechanical characterization. Then, the numerical models presented in this study were based on the elements characterized experimentally.

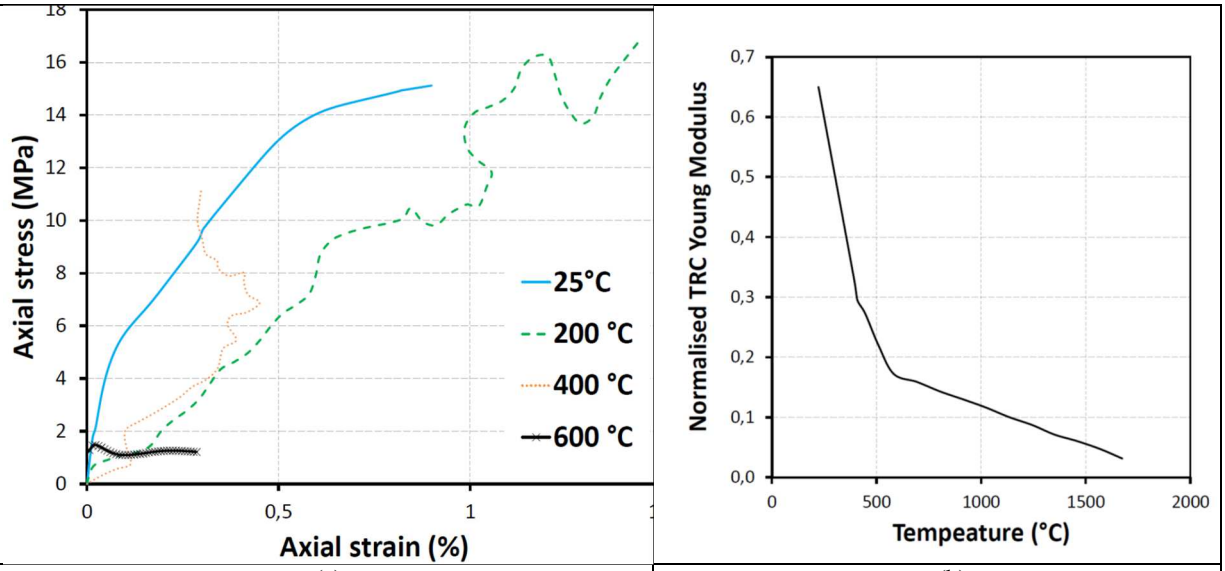

(a) (b)

Fig. 8. Thermomechanical behaviour of TRC for different elevated temperatures: (a) Experimental results obtained by [50]; (b) Evolution of normalised Young modulus of TRC as function of temperature.

3.4. Damage criterion and numerical implementation of the input data

The steel and concrete were assumed to be elasto-plastic materials.

3.4.1. Concrete

The plastic law of concrete was implemented using the Buyukuzturk criterion [52]. This criterion's plasticity surface, as given by Eq. (5), is very similar to the often-used Drucker-Prager's criterion in elasto-plastic analyses of concrete.

$$f = \beta \sqrt{3}\sigma J_1 + \gamma J_1^2 + 3J_2 - \sigma^2 \quad \text{[52]} \quad (5)$$

where f is the surface of the criterion, σ is the limit defined by the user, J_1 is first invariant of the stress tensor, and J_2 is the second invariant of the stress tensor.

Once the natural plasticity surface of the concrete was identified, a selection process to choose the best fitting plasticity surface available in the MARC MENTAT software (i.e., FE software) was performed. Figure 9a shows a comparison between an experimental plasticity surface of concrete [53] (Kupfer et al.; continuous line) and the numerical plasticity surface of the Buyukuzturk criterion [52]. Based on the evolution of the concrete's behaviour in tension with respect to the temperature, a corresponding softening plasticity law was implemented. This law was defined in two dimensions (i.e., the equivalent plastic strain and temperature). It should be noted that the stress-strain laws of concrete in tension were selected to incorporate the behaviour of the concrete, because failure occurred in the lower part of the RC beams tested in a flexural configuration. Moreover, the numerical results did not show any plastic behaviour in the portion of the beams in compression (i.e., the superior part of the beam). Figure 9b illustrates the softening law implemented for the concrete.

3.4.2. Steel

Steel was implemented in the numerical model via the Von-Mises plasticity surface (Fig. 10a). Once the volume of the elastic behaviour delimited by the plasticity surface was exceeded, plastic behaviour was initiated in accordance with the plasticity law Fig. 10b based on Fig. 7a.

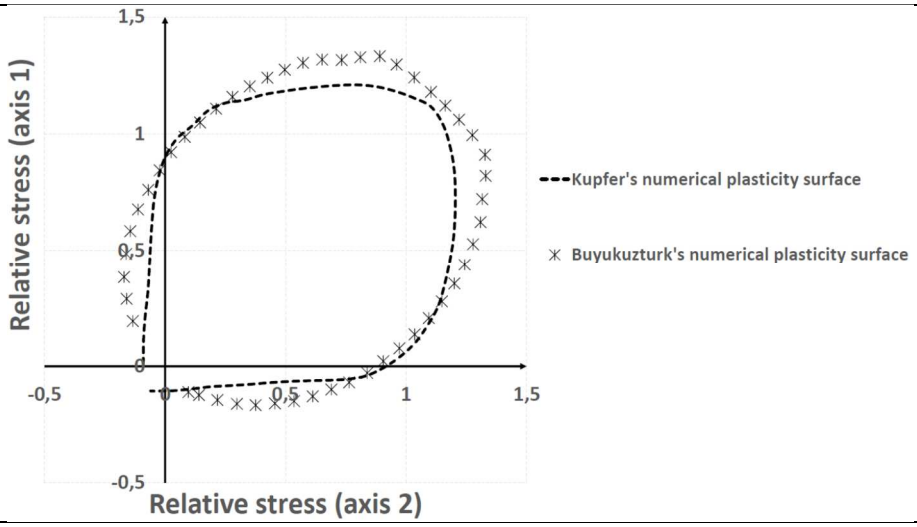

(a)

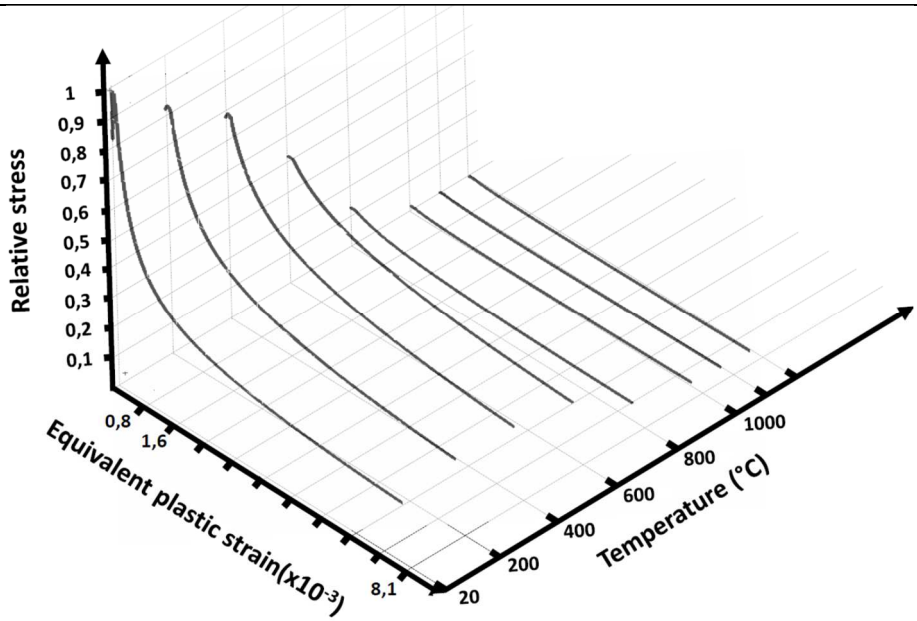

(b)

Fig. 9. (a) Plasticity surfaces of concrete according to the Kupfer criterion [53] (Kupfer, continuous line) (Kupfer et al.) and Buyukuzturk criterion (filled circle symbols) [52] (selected for the concrete in this study); (b) Evolution law of the concrete implemented in the MARC MENTAT software: concrete stress evolution as function of the equivalent plastic deformation in tension and temperature.

303

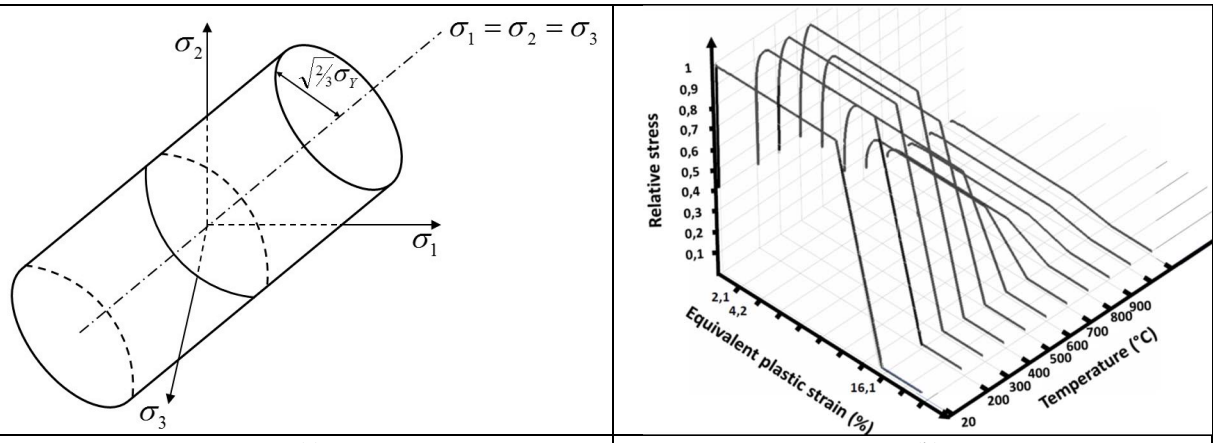

(a) (b)

Fig. 10. (a) Plasticity surfaces (i.e., surface delimiting the maximum elastic stress in a constrained space) of steel according to the Von-Mises plastic criterion [54]; (b) Evolution plastic law of the steel implemented in the MARC MENTAT software (evolution as a function of the equivalent plastic strain and temperature)

304

305 *3.4.3. TRC*

306 It is important to know that the unidirectional mechanical behaviour of a TRC along the longitudinal
307 direction can be subdivided into three or four zones ([8], [18], [10], [55] and [56]). The first zone (i.e., the first
308 slope) is a reversible linear phase. Once this linear zone is exceeded, damage and other phenomena start
309 occurring. In light of this behaviour, the TRC is considered to be an elasto-plastic material. It should also be
310 noted that the TRC composite is an anisotropic material owing to the constitutive material's disposition.
311 In this study, the TRC composites were attached to the bottom surface of the RC beams for flexural
312 strengthening. Therefore, these composites were loaded in tension only along their longitudinal direction.
313 Considering the unidirectional longitudinal loading of the TRC in this study, a Von-Mises criterion was used to
314 incorporate the TRC's mechanical plastic behaviour in the model. It should be noted that the Von-Mises criteria
315 is used for isotropic materials; however, it can be used to represent the plastic behaviour of the TRC under
316 unidirectional longitudinal mechanical loads. In order to assess the reliability of this choice, a literature review of
317 TRC strengthening on flexural settings was performed. The complex anisotropic mechanical behaviour of TRC
318 has been noted as a challenging aspect for authors throughout the numerical literature. At ambient temperatures,
319 a few authors ([57] and [17]) opted for an elastic model. These studies resulted in a good agreement between the
320 numerical and experimental mechanical results. Other studies ([58] and [59]) on TRC strengthened sandwich
321 beams corroborated those findings as long as the TRC was used in simple flexural bending conditions. An
322 isotropic plasticity model as tensile concrete damage plasticity (CDP) in the Abaqus software resulted in good
323 agreement with the experimental results. Based on these findings, an elastic zone was created using an isotropic
324 Von-Mises plasticity surface. Once the elastic zone of the TRC was exceeded, plastic behaviour was initiated.
325 This plastic behaviour was governed by a plastic law (see Fig. 11) extracted from the stress-strain behaviour of
326 the TRC used in this study (see Fig. 8a). The values of the Young's modulus of the studied TRC as function of
327 temperature (Fig. 8a) (i.e., the first slopes of the curves, which were also the elastic parts) were extracted and
328 implemented as a normalised Young's modulus curve with respect to the temperature (Fig. 8b).
329 The goal of the elastoplastic models, in the framework of this study, is to confer a realistic thermomechanical
330 behaviour to the modelled materials. This was done in order to establish an optimization tool and not a model
331 strictly reflecting the thermomechanical behaviour at any scale (e.g.: cracking behaviour). Taking this into
332 account, an elasto-plastic model can represent the thermomechanical behaviour of the TRC at a certain extent.
333 Moreover, the level of sophistication of the model is in line with the objectives assigned to this tool
334 (optimization, evaluation of major behaviour trends).
335

336 *3.4.4. Steel/concrete contact law*

337 Some authors [61] have explored the incidence of the steel/concrete contact law and concluded that its effect
338 on a structural scale was rather negligible for RC beams under mechanical and fire loads. The authors also

reported that the degradation of the steel/concrete contact law occurred simultaneously with the degradation of the mechanical properties of the steel, thereby creating a compensation effect. Consequently, a perfect contact law was implemented between the steel and concrete.

3.4.5. Concrete/TRC contact law

To the best of the authors' knowledge, only Tetta et al. [8] has addressed the behaviour of TRC strengthened RC beams subjected to elevated temperatures. Even though the mechanical contributions of the TRC to the RC beams were assessed in a shear configuration (U-wrapping and side bonding) for constant elevated temperatures, some conclusions could still be drawn. This experimental study showed that the mechanical failure of the specimens occurred predominantly at the concrete coating to which the TRC was attached. Failure rarely occurred at the concrete/TRC interface. For this reason, the concrete/TRC bond was assumed to be perfect in the numerical study. It should also be noted that further experimental tests should be conducted on this matter to ascertain the validity of this hypothesis; however, in the current study, no experimental tests were performed.

4. Numerical model results

4.1. Numerical models of the specimens modelled

Once the mechanical loads were fully applied, the thermal load was applied to the surface of the models as described in Table 1 (see "Thermal load"). The thermal flux was applied as the external air temperature surrounding the models. Table 2 shows the number of finite elements used for every modelled specimen. Figure 12 shows the numerical models of the modelled specimens for different configurations without TRC strengthening. The lateral section of Specimen 1 is shown in Fig. 12a, the longitudinal section of Specimen 1 is shown in Fig. 12b, the lateral section of Specimen 2 is shown in Fig. 12c, and the longitudinal section of Specimen 2 is shown in Fig. 12d. Figure 13 presents the numerical models of the modelled specimens strengthened with TRC in different configurations. The lateral section of Specimen 1 with one layer of TRC is shown in Fig. 13a, the lateral section of Specimen 1 with two layers of TRC is shown in Fig. 13b, the lateral section of Specimen 1 with three layers of TRC is shown in Fig. 13c, the longitudinal section of Specimen 1 with one layer of TRC is shown in Fig. 13d, the longitudinal section of Specimen 1 with two layers of TRC is shown in Fig. 13e, and the longitudinal section of Specimen 1 with three layers of TRC is shown in Fig. 13f.

366

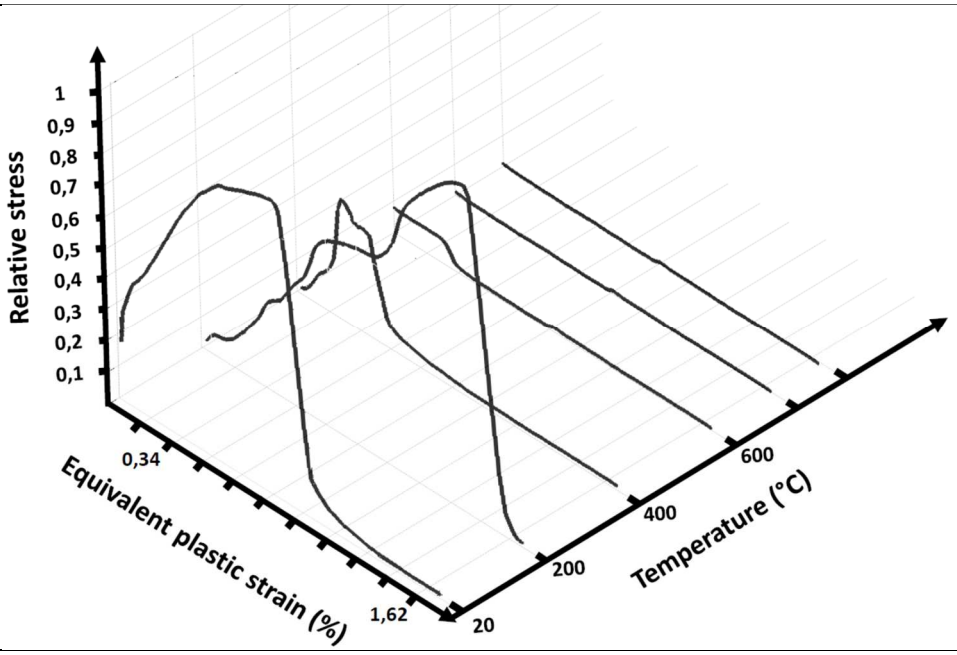

Fig. 11. Evolution of the plastic law of the TRC implemented in the MARC MENTAT software (Plastic law evolves as a function of the equivalent plastic strain and temperature)

367
368
369 Table 2 Number of elements in the numerical models built for Test Specimens 1 and 2

	Configuration	Steel	Concrete	TRC
Test model (Specimen 1)	Reference beams (Without TRC) (see Figs. 12(a)–12(b))	72	1548	None
	With TRC (see Figs. 13(a)–13(d))	72	1548	140
Test model (Specimen 2)	Without TRC (see Figs. 12(c)–12(d))	100	980	None

370
371

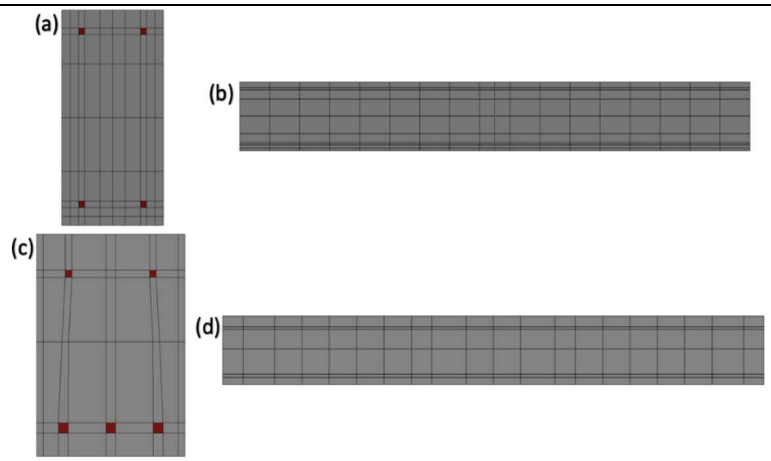

Fig. 12. Numerical models of the modelled specimens: (a) Lateral section of Specimen 1; (b) Longitudinal section of Specimen 1; (c) Lateral section of Specimen 2; and (d) Longitudinal section of Specimen 2

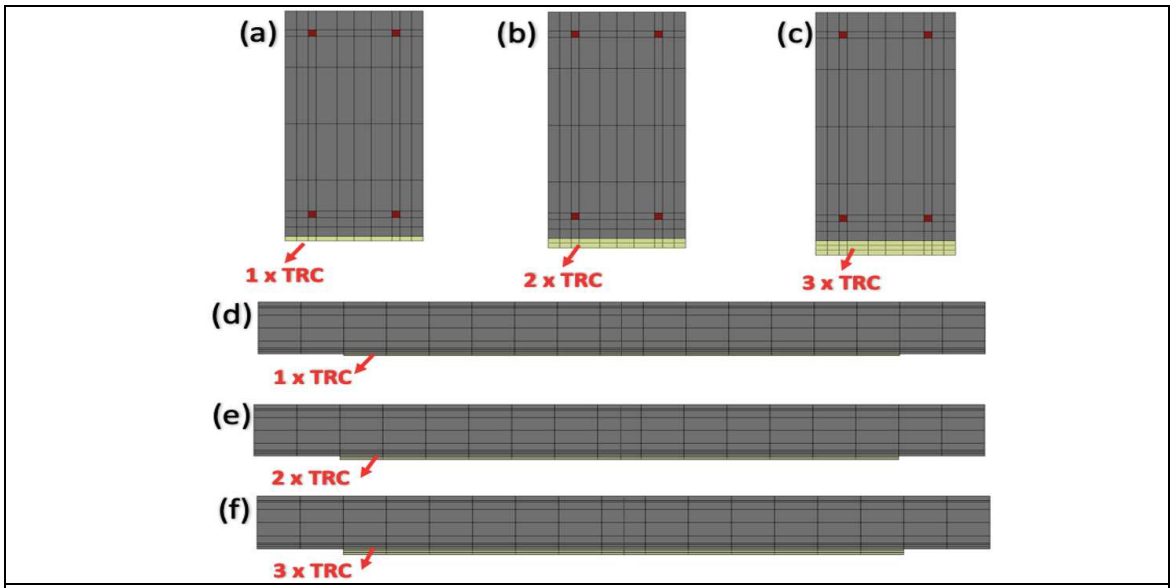

Fig. 13. Numerical models of the specimens modelled: (a) Lateral section of Specimen 1 with one layer of TRC; (b) Lateral section of Specimen 1 with two layers of TRC; (c) Lateral section of Specimen 1 with three layers of TRC; (d) Longitudinal section of Specimen 1 with one layer of TRC; (e) Longitudinal section of Specimen 1 with two layers of TRC; (f) Longitudinal section of Specimen 1 with three layers of TRC

4.2. Thermal results

The evolution of the temperature was the driving factor of all the thermomechanical phenomena. Therefore, as a first step, the numerical thermal fields were compared to the experimental temperature results in order to validate the thermal model. Figures 14 and 15 show the numerical and experimental temperatures measured at different depths in the mid-span section of Specimens 1 and 2.

The following conclusions were drawn from the results:

- The nearer we got to the heat-exposed surface, the less precise the model appeared to be. This was mainly attributed to the slight differences between the numerical and experimental thermal boundary conditions.
- Aside from the details previously highlighted, the numerical thermal results showed good agreement with the experimental measurements. This evidence emphasised the accuracy of the thermal models that incorporated the intrinsic thermal properties of concrete and steel as featured in Eurocodes 2 and 3.

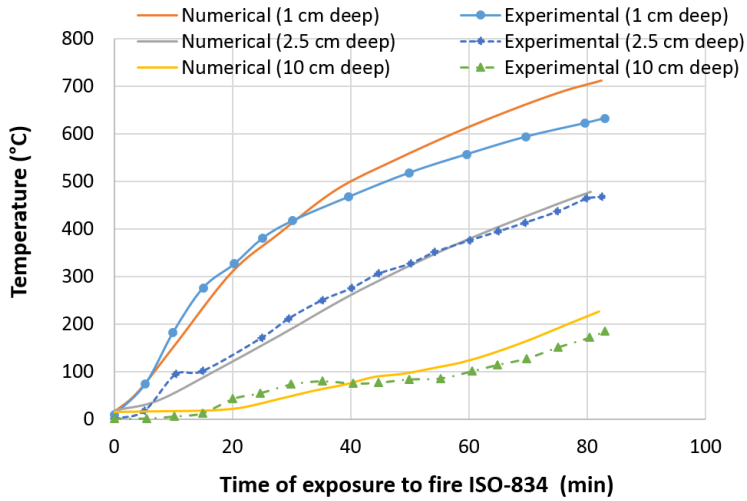

Fig. 14. Numerical-experimental comparison of the temperature fields of Specimen 1 without TRC strengthening (model shown in Figs. 12a and 12b); experimental results obtained from [39]

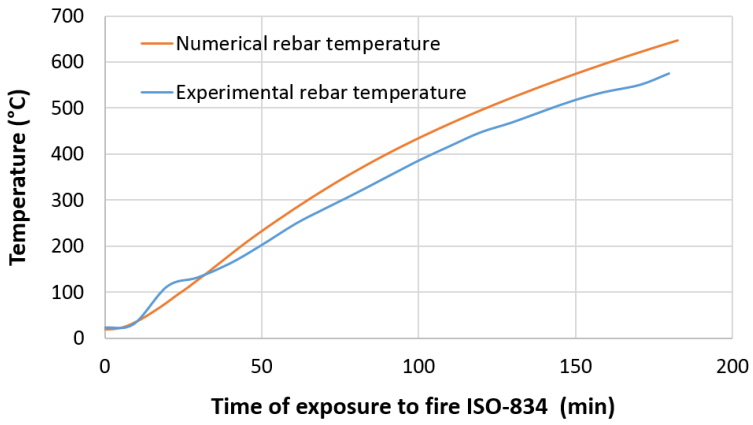

Fig. 15. Numerical-experimental comparison of the temperature fields of Specimen 2 without TRC strengthening (model shown in Figs. 12c and 12d; experimental results obtained from [40]

4.3. Thermomechanical results

Once the thermal study was validated, a thermomechanical analysis based on the study was performed. The mid-span deflections of Specimens 1 and 2 are shown in Figs. 16 and 17, respectively. It should be noted that the mid-span deflection is a general indicator (i.e., structural indicator) of the thermomechanical performance, although it is not a proper indicator of the mechanical state of RC beams.

Some of the conclusions drawn from the results shown in Figs. 16 and 17 are as follows:

- Figs. 16 and 17 show that the deflections with respect to time of the exposure to fire were in a good agreement for both the numerical and experimental values.
- The inflection points in Figs. 16 and 17, or the points where the deflection slope changed, denote the last portion of mechanical energy of the steel and concrete (i.e., the failure point of the RC beams). The failure prediction of the numerical models was always within 10 min of the experimental failure.
- It be noted that the steel/concrete perfect contact law hypothesis did not result in unrealistic mechanical behaviour.

Overall, the numerical predictions of the thermomechanical model were in good agreement with the experimental tests based on a comparison of the mid-span deflections.

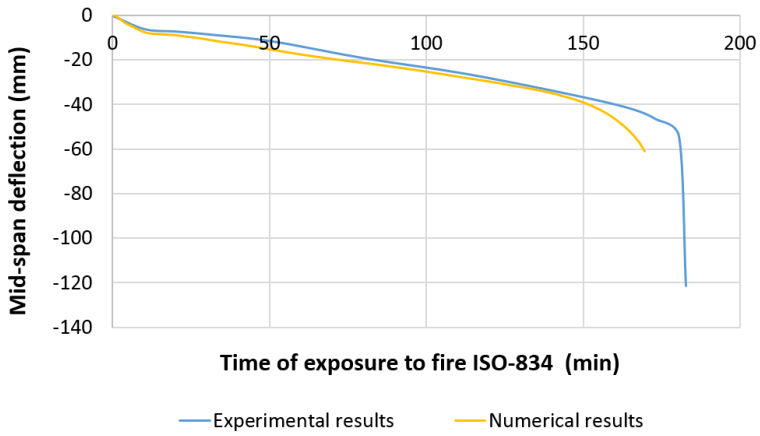

Fig. 16. Numerical-experimental comparison of the mid-span deflections of Specimen 1 without TRC strengthening (model shown in Figs. 12a and 12b); experimental results obtained from [39]

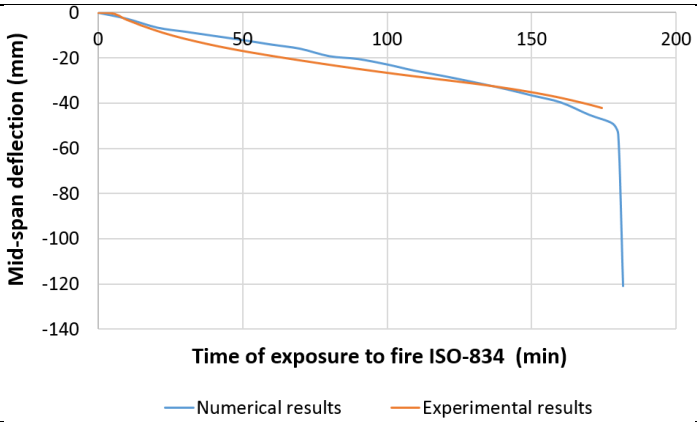

Fig. 17. Numerical-experimental comparison of the deflections of Specimen 2 without TRC strengthening (model shown in Figs. 12c and 12d); experimental results obtained from [40]

4.4. Parametric study: effect of the TRC thickness and thermal loading rate

In this section, the numerical studies of the RC beams strengthened with TRC layers are presented and discussed. The thermomechanical models of the unstrengthened RC beams validated in the previous section were also used for the numerical analysis in this section, but one to three layers of TRC composite were added to the bottom surface of the RC numerical models. It should be noted that fire and resistance tests must be conducted for the TRC strengthened RC structural elements in order to verify the findings of the numerical models (i.e., the RC beams strengthened by TRC) in this section. However, in this study, experimental fire tests were not carried out. The numerical modelling performed here was used to highlight the contribution and sensitivity of some of the parameters in order to better understand the potential of TRC materials, thereby allowing a finer experimental campaign framework in future studies. In addition, these models will increase the understanding of the damaging kinetics in scenarios both with and without TRC.

4.4.1. Effect of the TRC thickness

The purpose of this subsection is to assess effect of the TRC thickness on the global and local behaviour of the studied RC beams. The numerical thermomechanical model of Specimen 1 was chosen to assess this numerical study. Figure 19 shows the numerical results of the deflection as a function of the time of exposure to an ISO-834 fire for RC beams strengthened with one to three layers of TRC and a reference beam (i.e., one without TRC strengthening). It can be easily seen in Fig. 19 that the TRC contributed to an overall improvement in the behaviour of the RC specimens.

Fig. 18 shows the locations where the stresses were collected for all of the modelled configurations. The stresses, with respect to time, were collected in the steel rebar, concrete coating, and TRC in tension for all four configurations: (a), (b), (c), and (d). The pathline stresses were collected from the configuration without any TRC strengthening and the configuration with one layer of TRC (6 mm).

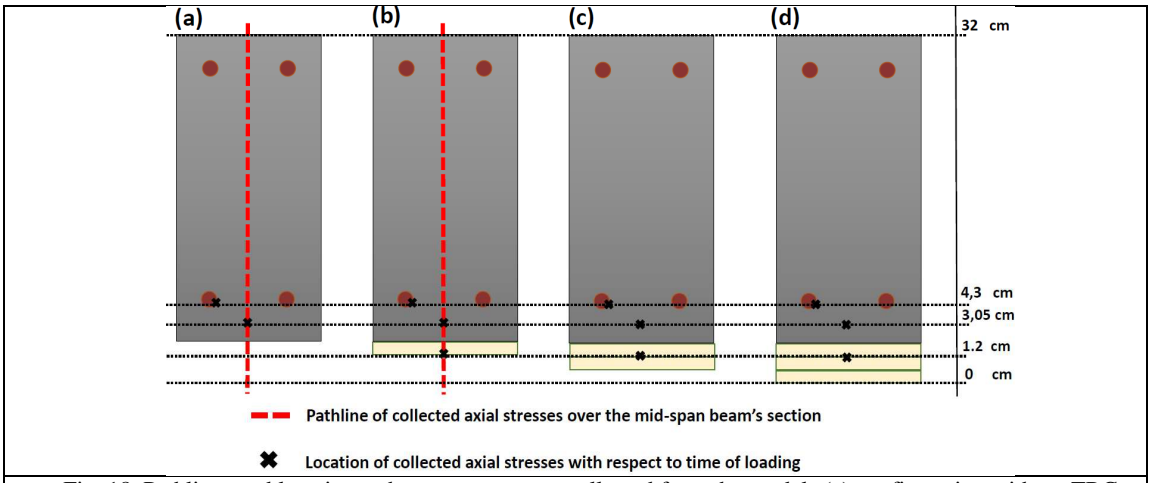

Fig. 18. Pathlines and locations where stresses were collected from the models (a) configuration without TRC strengthening, (b) configuration with one layer of TRC (6 mm), (c) configuration with two layers of TRC (12 mm), and (d) configuration with three layers of TRC (18 mm)

Fig. 19 clearly shows that adding layers of TRC to an RC beam improved the performance against both the mechanical and thermal loads. During the mechanical loading process, a slight mechanical contribution was provided by the TRC in the form of a smaller deflection rate). However, the effect of the TRC was more pronounced during the thermal loading. In fact, its effect manifested on two levels. First, the addition of more layers of TRC delayed the failure of the RC beams by roughly 7 min for each additional layer. The second effect was a less pronounced deflection rate.

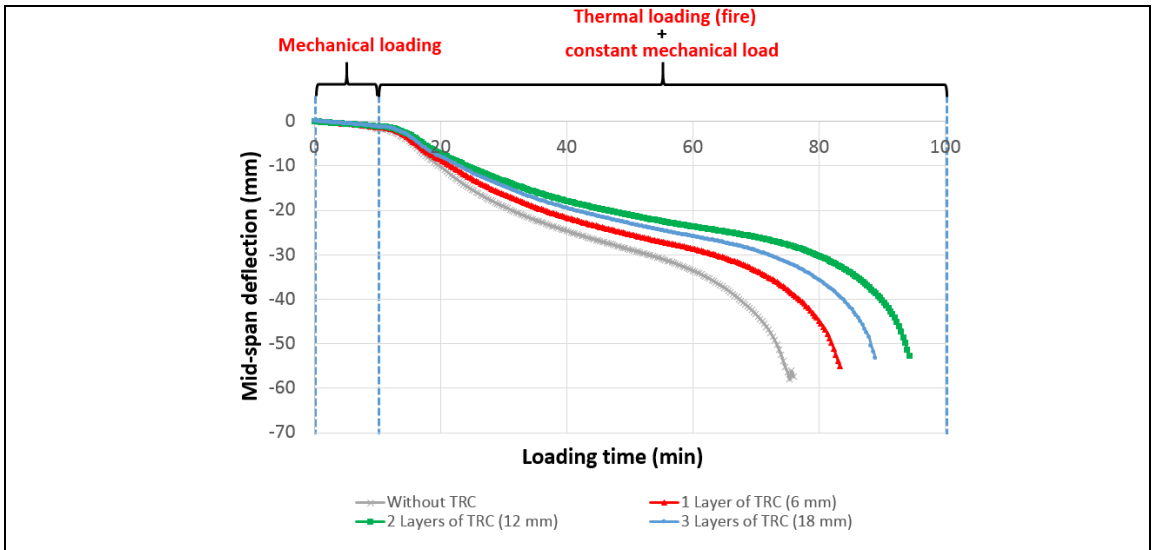

Fig. 19. Numerical deflections of Specimen 1 (strengthened with zero to three layers of TRC) with respect to the loading time (mechanical and thermal loads)

As was stated in Section 3.4.5, failure of the TRC strengthened RC elements occurred in the concrete coating where the TRC composite was bonded. Therefore, to increase our understanding of the thermomechanical phenomena, special focus was placed on the axial stresses in the lower mid-span part of the RC beams, as it was the most used part. Figure 20 shows the evolution of the axial stresses in the concrete coating and tensile steel for both unstrengthened and TRC strengthened RC beams.

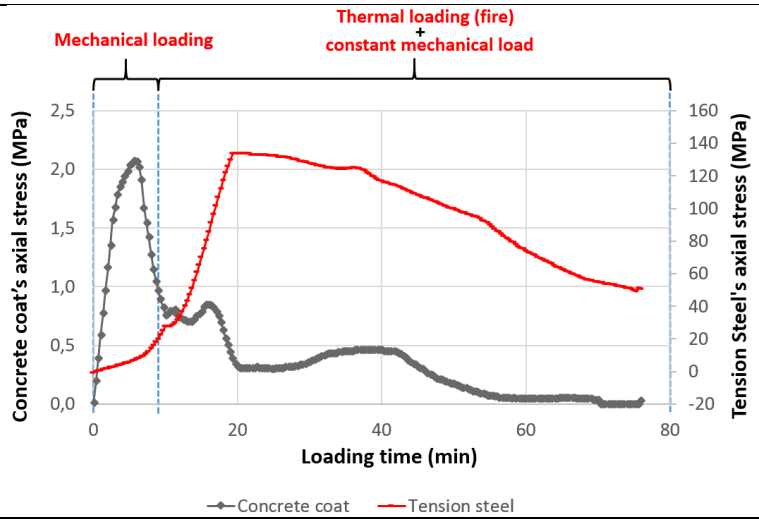

Fig. 20. Numerical axial stresses in Specimen 1 (without TRC) with respect to the loading time (mechanical and thermal loads)

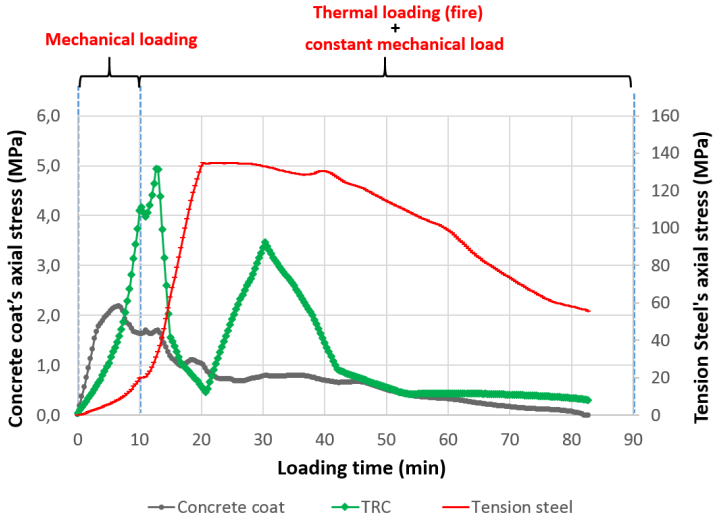

Fig. 21. Numerical axial stresses of steel, concrete coating, and TRC (in the lower mid-span part of the RC beam) in Specimen 1 (strengthened with one-layer, i.e., 6 mm, of TRC) with respect to the loading time (mechanical and thermal loads)

Figure 20 shows the evolution of the axial stresses with respect to the loading time. The mechanical load was applied gradually over the first 10 min. It can be seen that the applied load exceeded the service limit state as the stresses in the concrete coating exceeded the reversible linear phase of the material. Consequently, the tensile steel rebar compensated for the lost tension with an increase in their axial stresses. It should be noted that the Eurocode 2 design rules corroborate the fact that the mechanical load applied to the Specimen 1 RC beam places the beam between the service limit state and ultimate limit state. Figure 22 also corroborates this condition as the axial stresses in the mid-span section at 10 min (i.e., the beginning of the thermal load) are not linear throughout the concrete section. This suggests that the lower part of the section has passed beyond the elastic limit of the material. Once the mechanical load was fully applied, it was kept constant and a thermal load (i.e., the ISO-834 load) was applied to the specimens.

In Fig. 20, the initial stress status of the RC beam was quickly disturbed in the first 8 min of heat exposure. The concrete coating lost roughly one third of its initial axial stress (at 20 °C) due to the temperature evolution. This stress loss was attributed to a combination of the regression in the mechanical properties and the thermal expansion of the lower part of the beam. During the time period in which the concrete's axial stress decreased, the steel's axial stress rose until minute 22, where it peaked. After the initial stress recovery of the concrete coating (seen at minute 17), it ultimately decreases. The stress in the steel and concrete continued to decrease until minute 45, where a severe decrease in the axial stress of the concrete is noted. This resulted in an increase in the deflection rate after minute 45 (see Fig. 19). The axial stresses in the concrete and steel continued to

decrease until minute 75, where the steel temperature exceeded 500 °C, and the stress in the concrete coating reached zero, which caused the RC beam to fail.

For the TRC (6 mm) strengthened RC beam (Fig. 21), the axial stress history was slightly different owing to the mechanical contribution of the TRC.

The following conclusions were drawn from the mechanical loading phase (Fig. 21):

- The mechanical loading phase exhibited some similarities to the unstrengthened specimen (i.e., without TRC, see Fig. 20) although the TRC addition contributed to the consolidation of the concrete coating by allowing it to have a better mechanical performance at the end of the mechanical loading phase (see minute 10 in Figs. 22 and 23).
- The following conclusions were drawn from the thermal loading phase (Fig. 21): At first, a decrease in the axial stress occurred in the concrete coating and TRC. Thereafter, the axial stress in the steel increased (stress compensation) until minute 22. This phenomenon was also noted for the configuration without TRC (Fig. 20).
- The mechanical contribution of the TRC peaked at minute 31, then regressed sharply until minute 44.
- The axial stress of the steel started decreasing at minute 21 due the temperature.
- All of the constitutive materials continued to lose their axial strength until the concrete coating reached a zero-stress state, which caused the specimen's failure.

It should be noted that the axial stress of the TRC was dependent on the properties of the concrete coating to which the TRC was attached. Therefore, additional investigations focused on this relationship should be carried. However, the achievement of a zero stress state in the concrete at minute 77 (Fig. 21), which caused the failure of the strengthened beam, was in a good agreement with the previous study [8], which reported that the predominant failure mode occurred in the concrete coating to which the TRC was bonded.

Figures 22 and 23 show the numerical axial stresses through the vertical axial axis of the mid-span section of the configurations (see Figs. 18(a) and (b)) without TRC strengthening (Fig. 22) and with one layer (6 mm) of TRC strengthening (Fig. 23). These figures show the axial stresses at minute 0 (i.e., prior to mechanical loading), minutes 10 (i.e., the end of mechanical loading and beginning of thermal loading), and minutes 80 and 82 (i.e., failure).

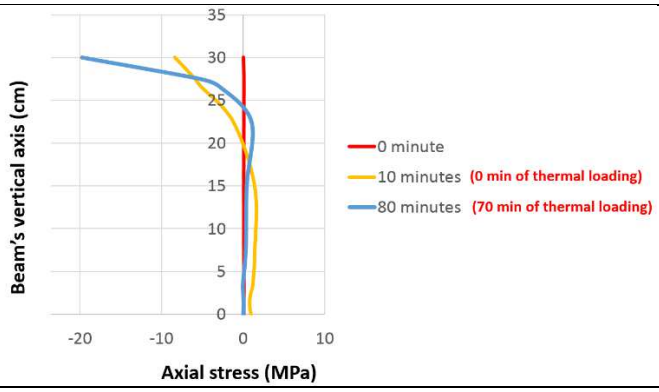

Fig. 22. Numerical axial stresses of Specimen 1 (without TRC strengthening) over the vertical symmetrical axis of the mid-span section (Fig. 18(a))

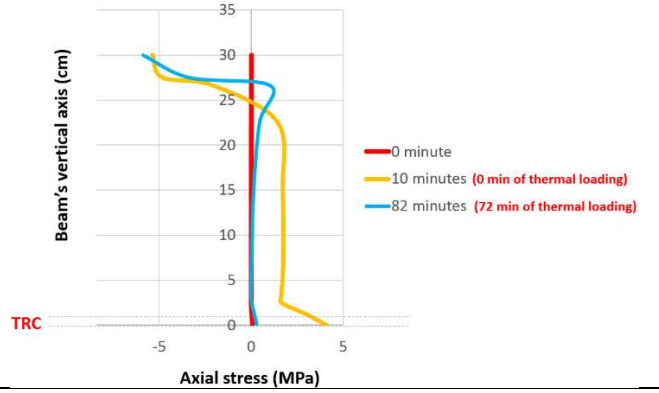

Fig. 23. Numerical axial stresses of Specimen 1 (with one layer of TRC strengthening (6 mm)) over the vertical symmetrical axis of the mid-span section (Fig. 18(b))

To fully understand the local mechanical behaviour of the TRC strengthened RC beam, the elastic, thermal, and plastic axial strains (Fig. 24) were collected at the same locations where the axial stresses were collected (Fig. 21) (i.e., tensile steel rebar, concrete coating, and TRC).

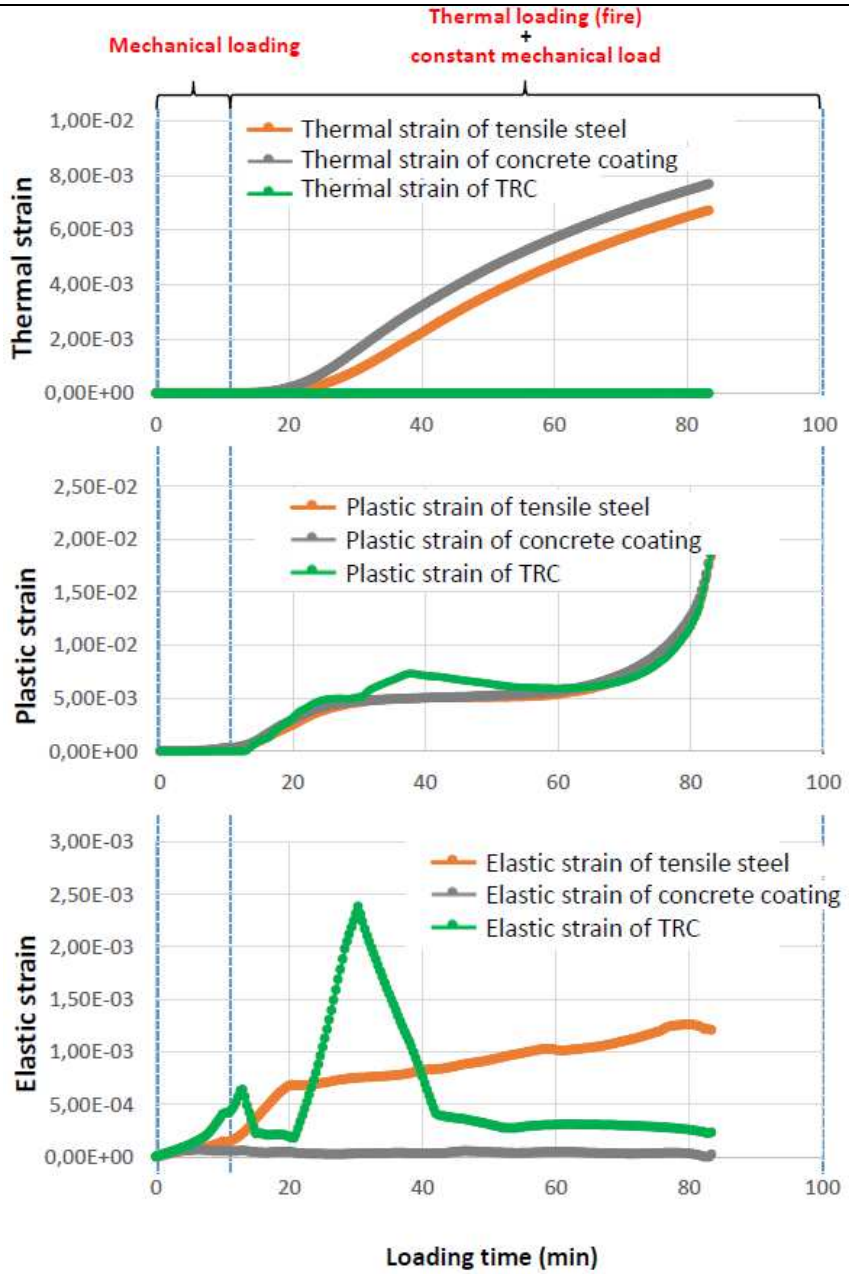

Fig. 24. Numerical axial strains of the steel, concrete coating, and TRC (in the lower mid-span part of the RC beam) of Specimen 1 (with one layer of TRC strengthening) with respect to the loading time (mechanical and thermal loads)

During the mechanical loading phase (Fig. 24), the following observation was made:

- A slight increase in the plastic strain of the concrete coating was noted. This corroborated the previous statement made regarding the mechanical load pushing the RC beam beyond the mechanical service limit state.

During the thermal loading phase (fig. 24), the following observations were made:

- From minute 10 to minute 17, a slightly differentiated increase in the thermal strains of the concrete and steel was noted. This differentiated thermal strain (i.e., concrete expands more than steel) helped to decrease the axial tensile stress in the concrete, while the axial stress in the steel increased (Fig. 21). Simultaneously, an elastic strain decrease was noted for the concrete, while the steel experienced an elastic strain increase. The plastic strain of all of the materials increased as a result of the temperature evolution.
- The axial elastic strain of the TRC decreased heavily during the first 10 min as a result of the thermal damage.
- At minute 20, the axial stress peaks of the steel began to decrease (Fig. 21). This led to an increase in the elastic strain of the TRC and a stress peak at minute 30.
- After minute 30, the mechanical contribution of the TRC decreased (i.e., less elastic strain and more plastic strain).
- After minute 42, the thermal and plastic strains began to increase a second time; thus explaining the axial stress releases (Fig. 21).

Now that the phenomena involved in the thermomechanical history are clear, focus is brought to the effect of the TRC thickness (i.e., the number of layers) on the overall thermomechanical behaviour. Figure 25 shows the effect of the number of TRC layers on the local mechanical behaviour of the reinforced configurations. The following conclusions were drawn:

Mechanical loading phase (Fig. 25):

- Strengthening an RC beam with additional layers of TRC helped the concrete coating remain consolidated and perform more efficiently (Fig. 25 (a)).
- The thickness of the TRC brought a slight mechanical contribution to the concrete coating and the tensile steel rebar during mechanical loading. In fact, compared to the unstrengthened RC beams (Fig. 25(a) and (b)), the steel rebar and concrete coating bore less axial stress in the configurations that utilised TRC strengthening.
- It should also be noted that during and at the end of the mechanical loading phase (Fig. 25(c)), the axial stresses in the TRC were more important for those configurations strengthened with fewer layers of TRC. Naturally, this was the result of the increase in the stress concentration that occurred due to the decrease in the TRC surface (for configurations with less layers).

Thermal loading phase (Fig. 25):

- Initial stress state of the concrete:
  The axial stress in the concrete coating should be less important for TRC strengthened configurations (i.e., those with a higher beam inertia), although this assumption would only be true for infinitely linear elastic materials. In this case, the concrete was a nonlinear material. As stated previously, the mechanical loads applied to the reinforced beam went beyond the service limit state defined in Eurocode 2. Therefore, the concrete coating was slightly damaged before the heat flux was applied to the beam. This explains why, at the beginning of the thermal loading phase (Fig. 25(a)), the axial stresses were more important for the configurations with more layers of TRC, as the TRC kept the concrete coating intact and consolidated under a mechanical load.
- Stress limit of the steel:
  - ✓ The increasing number of TRC layers caused the axial stress curves of the steel to shift down.
  - ✓ The axial stress peaks of the steel occurred at roughly the same time (minute 23), which emphasised the fact that the reduction in the steel stress was directly linked to a specific temperature point.
- Thermal effect:
  - ✓ In the first few minutes of the thermal loading phase, a peak of stress was noted for the concrete and TRC. It was also noted that this stress peak increased when the number of TRC layers increased. This was attributed to the stiffness of the TRC against the thermal expansion of the concrete.
  - ✓ After the first 7 min, the stress in the concrete coating and TRC decreased in all configurations (Figs. 25(a) and (c)). This phenomenon was caused by the reduction in mechanical properties, which led to a stress release in those parts of the beams.
  - ✓ The increase in steel stress was caused by a combination of the differentiated thermal expansion (between the concrete and steel) and the reduction in concrete properties as a result of the temperature.
  - ✓ The stress peak of the steel (Fig. 25(b)) occurred at roughly the same point for all of the configurations. This emphasised the fact that the steel stress limit was directly linked to the temperature evolution.

554 ✓ The second mechanical contribution of the TRC began at the stress limit of the steel rebar. It was noted
555 that this mechanical contribution grew larger and was delayed (in time) as the number of TRC layers
556 increased. This might due to the fact that a larger number of TRC layers acts as thermal shield for the inner
557 TRC layer (where the axial stresses were collected for Fig. 25(c)), which kept was kept sufficiently cool to
558 contribute in a delayed manner.

559 • Additional layers of TRC improved the concrete coating performance during the thermal loading phase
560 owing to the fact that the TRC layers kept it intact during the mechanical loading phase and the first few
561 minutes of the thermal loading phase.
562

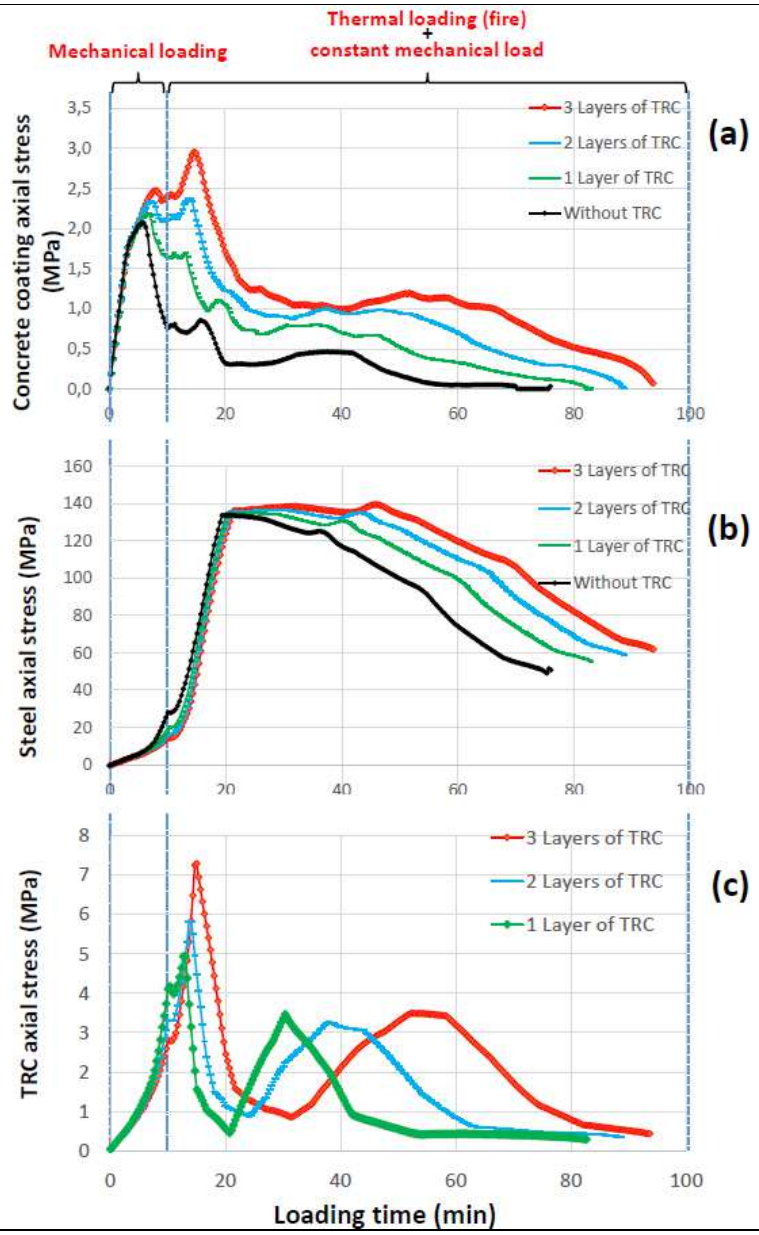

Fig. 25. Numerical axial stresses in the steel, concrete coating, and TRC (in the lower mid-span part of the RC beam) of Specimen 1 (without TRC, with one layer of TRC, with two layers of TRC, and with three layers of TRC) with respect to the loading time (mechanical and thermal loads)

563

The results of the analysis showed in this sub-section led to the following conclusions:

- Additional layers of TRC improved the stiffness of beams (i.e., the inertia of the beam's section increased). Therefore, the deflection as a function of the time of exposure to the thermal load decreased. Moreover, the thermal exposure resistance time was enhanced.
- TRC strengthening helped to keep the concrete coating consolidated, which allowed it to perform more efficiently during when exposed to the thermal load.
- The TRC strengthening provided a mechanical contribution during the mechanical loading phase.
- The TRC strengthening provided a second mechanical contribution (delayed) after the tensile steel rebar reached their stress limit.
- It should also be noted that the TRC layers also contributed at a thermal level by delaying the temperature evolution. Consequently, failure was also delayed.
- The mechanical contribution of the TRC was limited by two factors:
  - ✓ The TRC's properties regressed as the temperature increased.
  - ✓ The concrete coating on the bottom of the beam weakened with continued exposure to the thermal load, resulting in poor mechanical stress transfers between the RC beam and TRC.

4.4.2. Effect of the thermal loading rate

A numerical study was carried out on RC beams strengthened with one layer of TRC under a unique mechanical load but different heating scenarios. The thermomechanical models of the unstrengthened RC beams validated in Section 4.3 were also used for the numerical analysis in this section, but employed different heating rates. It should, again, be noted, that fire and resistance tests need to be performed for TRC strengthened RC structural elements in order to validate the findings of this study. However, experimental fire tests were not carried out as a part of this research.

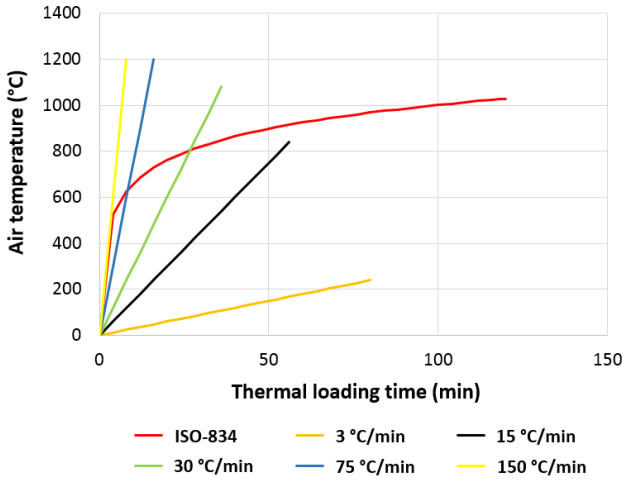

Fig. 26. Numerical model heating rates

In this numerical study, the ISO-834 heating rate was substituted with five different heating rates (see Fig. 26) (3 °C/min, 15 °C/min, 30 °C/min, 75 °C/min, and 150 °C/min)]. The purpose of this parametric study was to assess the thermomechanical effects of the heating rate on the global and local behaviour of the studied RC beams.

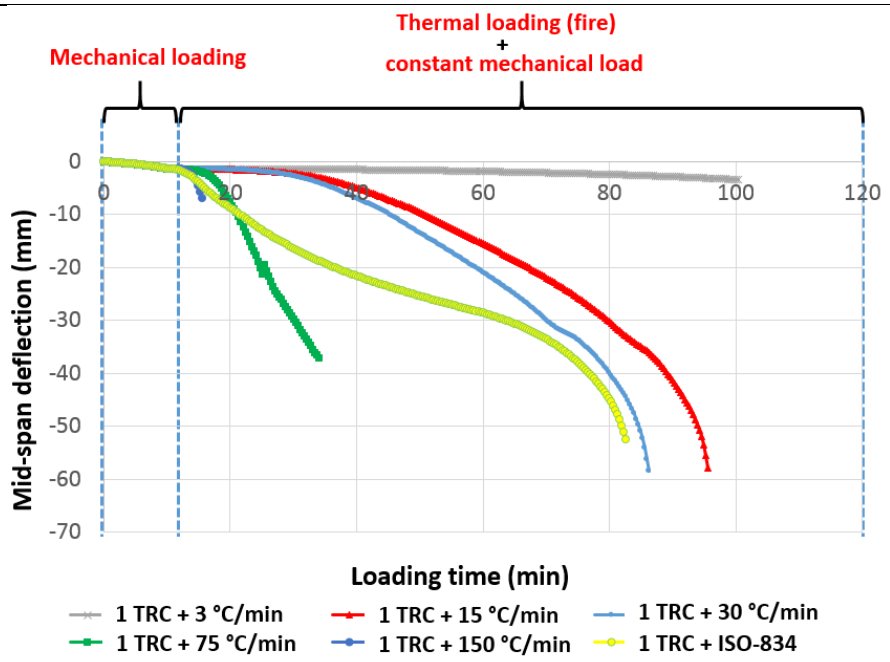

Fig. 27. Numerical model deflections of Specimen 1 (strengthened with one layer of 6 mm thick TRC) with respect to the loading time (mechanical and thermal loads)

Figure 27 shows the numerical model deflections of Specimen 1 (strengthened with one layer of 6 mm thick TRC) with respect to the time of exposure to the mechanical and thermal loads for different heating rates that varied from 3 °C/min to 150 °C/min and the ISO-834 heating rate (Fig. 26). Figure 27 present the numerical results of Specimen 1 strengthened with one layer (6 mm) of TRC for the evolution of the axial stress of the (a) steel, (b) concrete coating, and (c) TRC as a function of the loading time. From the results obtained and presented in Figs. 27 and 28, the following points were observed:

- As expected, a lower heating rate led to a lower deflection rate over time.
- Excluding the 3 °C/min heating rate that was too slow to fully affect the specimen within the truncated analysis time (the curve was shorted to 100 minutes), an important conclusion was noted. The ISO-834 heating rate failed at roughly the same deflection as the 15 °C/min and 30 °C/min rates. Based on this finding, it can be stated that, within the latter heating rate range, the heating rate itself did not affect the mechanical history of the failure besides delaying it. Figure 28 supports this finding as the heating rates appeared to have a delayed effect on the axial stress histories of the concrete and TRC. The same flexural behaviour was observed in [37], where RC beams were loaded mechanically and then tested on their resistance to fire at different thermal loading rates (ASTM E119 and a long, severe heating rate). This experimental study showed that a severe heating rate resulted in steeper deflections over time and an earlier failure than the ASTM heating rate. However, the failure occurred at the same deflection as ASTM E119, and the findings of the study with the long, severe heating rate [38] for slower and faster heating rates than ASTM E119 also corroborated the results in Fig. 27.
- It must be noted that higher heating rates (i.e., 75 °C/min and 150 °C/min), and with the support of Figs. 27 and 28, the numerical calculations appeared to conclude before the axial stresses reached zero. This was most likely due to numerical convergence issues.

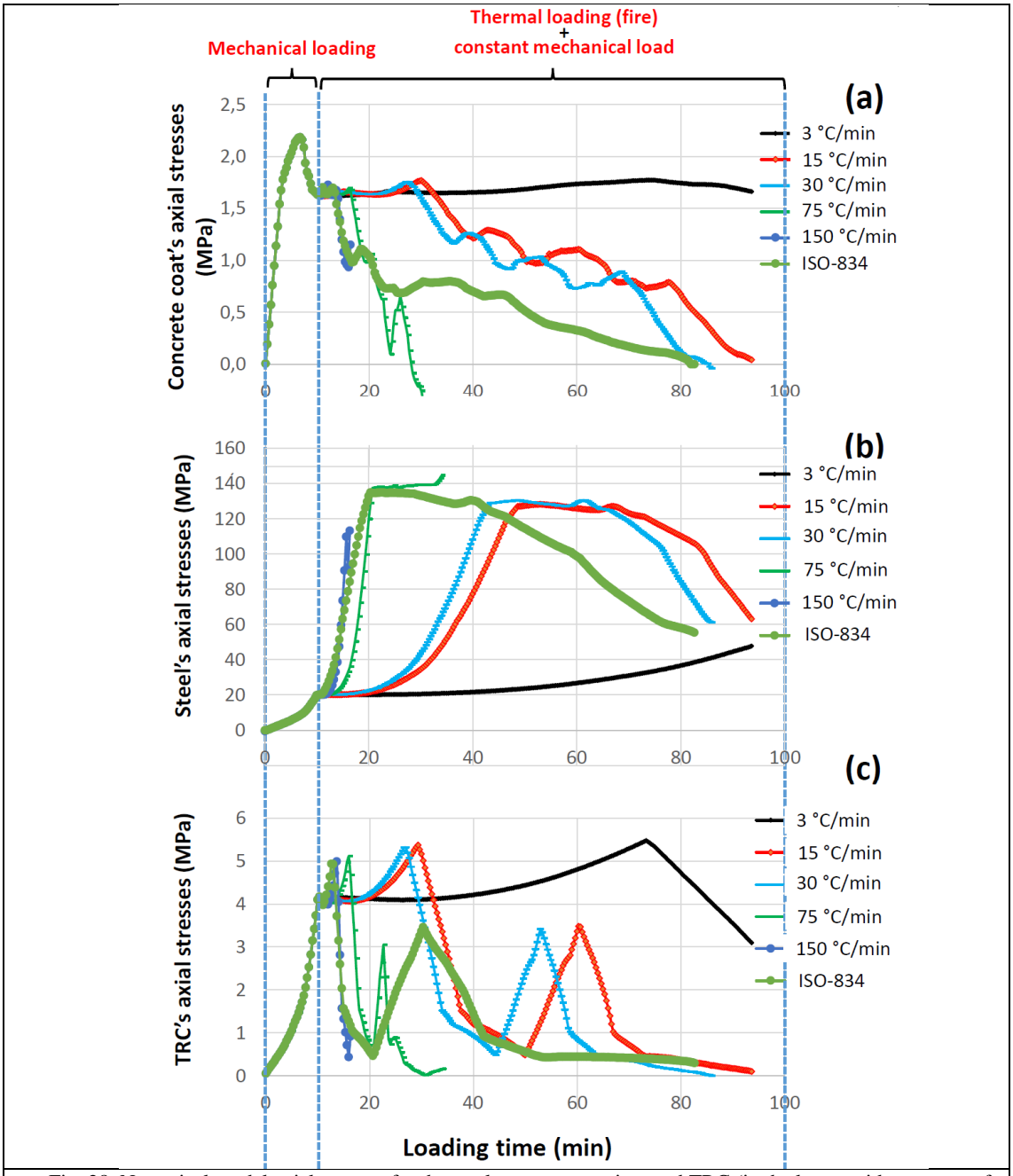

Fig. 28. Numerical model axial stresses for the steel, concrete coating, and TRC (in the lower mid-span part of the RC beam) of Specimen 1 for five heating rates with respect to the loading time (mechanical and thermal loads)

It should be noted that Fig. 28 illustrates the mechanical history findings of the previous section (i.e., Section 4.3.1 Effect of the TRC thickness). The first axial stress peaks of the steel (Fig. 27(a)) (at minute 10) coincided with the second mechanical contribution of the TRC (Fig. 27(c)).

The results showed in this sub-section led to the following conclusions:

- The heating rate of a TRC strengthened RC beam within the ISO-834 range did not change the thermomechanical history of the constitutive materials. However, it delayed the thermomechanical effects.

4.4.3. Residual capacity

After a fire, the cooling of the reinforced concrete elements is associated with a change of the mechanical properties of the constitutive materials. Steel reinforcements can restore their full mechanical capacity before a temperature of 600°C, however, above 600°C, only 90% of their capacity is recoverable after cooling [62]. On the other hand, concrete experiences an additional degradation of its mechanical properties during cooling, a phenomenon caused by cracks that develop in the material.

Eurocode 2 [44] as well as other normative references such as the Japanese standard (AIJ fire resistive materials' guideline, 2009) evaluate the residual strength of a reinforced concrete element based on minimum cross-sectional dimension tabulations or the time it takes for the 500°C front to reach the critical concrete cross-section, and then the strength of the steels is calculated based on the corresponding maximum temperature at that time. Furthermore, [62] reported that monitoring the evolution of the 500°C front was not sufficient to assess the residual strength of the concrete. Raouffard et al. [62] also stated that the reason behind this was that the cooling phase induced a 30% decrease in the residual fire resistance of a reinforced concrete beam. This decrease was related to the development of cracks in the concrete during cooling. The European standard [63] defines failure criteria based on the deflection of the fire-rated reinforced concrete beam (see the equation 6).

$$d_{iso} = \frac{l^2}{400.d} \quad (6)$$

Where d_{iso} is the ISO-834 fire deflection limit, l is the clear span of the beam and d is the distance from the extreme fiber on the cold design compression zone to the extreme fiber on the cold design tension section.

Moreover, the literature is in common agreement regarding the impact of steel temperature on the mechanical resistance during and after a fire. Raouffard et al. [64] numerically assessed the sensitivity of the residual strength of (RC beams after a fire) to some structural parameters such as the level of mechanical loading. It was concluded that the higher the mechanical loading, the lower the residual resistance of the RC element after a fire. The causal link lies in the mechanical states of the tension steel rebars and the concrete coat which are more stressed for higher mechanical loading levels, thus, the evolution of temperature has more impact on the degradation of the yield strength and the plastic strains of the constituent materials (see Fig. 10b). Therefore, in order to accurately assess the residual mechanical strength of RC beams, it seems natural to include the effect of some parameters such as the heating scenario, the temperature of the tensile steel, the level of mechanical loading [64].

Taking into account the elements presented above, the assessment of the contribution of the TRC to improve the residual mechanical strength of the RC beams will be based on the evolution of the deflection, the temperature in the RC section and the axial stress of the concrete coat and steel rebars. From a thermal perspective, the TRC is too thin (6 mm) to take its heat insulation effect into consideration, therefore, its thermal preservation of the residual strength is at best of little importance, this is in addition to the fact that the TRC has a higher thermal conductivity than concrete considering the carbon based textile grids. This study showed that the addition of TRC reinforcement layers induced stress reduction in the tension steel rebars (see Fig.25(b)) at 10 minutes. Thus, considering these elements, the potential effect of TRC on the residual strength of a RC beam can be attributed to its ability to reduce the axial stresses of the steel rebars and the concrete coat, thus reducing the severity of fire-induced mechanical damage [64]. The fire deflection limit established by Eurocode 2 is estimated to be 75 mm for specimen 1. From the results of section 4.4.1 and 4.4.2, it appears that the addition of TRC layers delays the effect of fire, which is in agreement with the elements explained above.

One can add that the residual strength of the TRC strengthened RC beams would also depend on the residual strength of the TRC, which remains significant even after exposure to fire [60].

It remains, however, important to emphasize that the exclusively deductive nature of the above paragraphs must be reinforced by parameter sensitivity assessments to ascertain the post-fire contribution of the TRC to RC beams.

5. Conclusion

The objective of this study is to provide an optimization tool for TRC strengthened reinforced concrete beams. Within the limits of the hypotheses on which this numerical model is based, this tool will allow to draw indications that are capable of limiting the number of experimental tests envisaged. Also, the understanding provided by this study will evolve with the experimental tests envisaged in the future. It is important to point out that the need to carry out an experimental validation is essential.

This paper assessed numerically the mechanical and thermal contributions of a new composite material, textile-reinforced concrete (TRC), to strengthen steel reinforced concrete beams in case of fire loading (ISO-834) and/or different thermal loading rates varying from 3 °C/minute to 150°C/minute. The numerical models were developed through this study, it was concluded that TRC could be a good strengthening solution for steel reinforced concrete beams in case of fire or subjected to elevated temperatures with different heating rates.

The findings of this study are shown below:

- Using the intrinsic thermal properties of concrete and steel, featured in the Eurocodes 2 and 3 in thermal analysis resulted in precise thermal fields for a reinforced concrete beam under fire (ISO-834 normalized fire curve)

TRC's thickness effect on global and local behaviour of RC beam is synthesized below:

- The mechanical contribution of the TRC strengthening led to a better thermomechanical performance against fire. The deflection and deflection rates of the reinforced specimens both decreased with the addition of the TRC. Thus, the failure of the RC beams during the ISO-834 heat exposure was delayed.
- During mechanical loading, TRC strengthening consolidates the concrete coat and therefore supports part of the axial stresses of the tension steel rebars and the concrete coat. This way, at the end of the mechanical loading, the stiffness of the embedding concrete is preserved.
- During the thermomechanical loading phase, the concrete coat that was preserved during mechanical loading shows higher tensile stresses. In addition, the TRC have additional mechanical contributions to the reinforced concrete beams during thermomechanical loading, particularly when the stresses of the tension steel rebars starts decreasing under heat.
- Naturally, reinforcement with additional TRC layers results in higher mechanical and thermal effects.
- TRC layers also provide thermal protection, therefore, all thermal effects are delayed, including failure.
- The literature showed that less stressed tension rebars lead to less mechanical damage during fire exposure. As seen through this study, TRC strengthening partly relieves tension steel rebars of tensile stresses at the end of the mechanical loading phase. This suggests that the TRC have the potential to improve the residual strength of RC beams after fire, this, in addition to its own mechanical residual strength.
- Concrete's bottom coat weakened with temperature exposure resulting in poor mechanical stress transfers between the RC beams and the TRC. Therefore, the thermomechanical contribution of the TRC is very dependent on the concrete coat's fire resistance.

Heating rate effect on global and local behaviour of RC beam is synthesized below:

- The evolution of axial stress of concrete coat, steel and TRC in the lower mid-span part of the RC beam as a function of the loading time (mechanical and thermal loading) for different thermal loading rates was numerically identified and analyzed.
- From 15°C/minute to 150°C/minute and ISO-834 heating rate, the heating rate did not affect the deflection r eached at failure nor failure's mechanical history of RC beam strengthened by one-layer-6mm TRC besides delaying it. These findings are consistent with the experimental conclusions found in the literature.

Compared with traditional Fiber Reinforced Polymer (FRP) material, TRC has two important advantages:

- During a fire, TRC/concrete interface is less sensitive with temperature than FRP/concrete interface.
- TRC does not emit toxic fumes such as FRP.
- TRC can potentially contributes to improve the residual strength of fire RC beams

Based on this work, some prospects can be drawn:

- This work provided a better understanding of the thermomechanical phenomena involved in a RC beam strengthened with TRC, therefore, a founded frame of experimental tests can be envisioned based on this work for a detailed analysis.
- Optimizing the thermomechanical potential of TRC strengthening by protecting it with thermal insulation materials.
- Solving the adherence problems (weakening concrete coat with fire) by setting up the TRC strengthening with an anchorage system.

The numerical models showed the contribution and sensitivity of two parameters (i.e., the TRC thickness and thermal loading rate) on the global and local behaviour of steel reinforced concrete beams. The findings of this numerical model increased our understanding of the potential of TRC material and will enable finer experimental campaigns in future studies. In order to valorise the full thermomechanical potential of TRC, further numerical work should be conducted along with new experimental tests to ascertain, complete, and validate the numerical findings of this study.

Acknowledgments

This research was performed with the financial subvention of the Public Investment Bank of France (BPI France) for the lot 6 "Design method & normative aspects" of the PRORETEX II research project. This project is a collaborative research project between four industrial partners (SULITEC - project leader, FOTIA, ER2I, CIMEO) and two academic partners (ENISE/LTDS, UCBL/LMC2).

References

[1] Shaikh F.U.A., Taweel M. (2015), "Compressive strength and failure behaviour of fibre reinforced concrete at elevated temperatures", *Advances in Concrete Construction*, **3**(4), 29283-293.
[2] Ponikiewski T., Katzer J., Kilijanek A., Kuźmińska E. (2018), "Mechanical behaviour of steel fibre reinforced SCC after being exposed to fire", *Advances in Concrete Construction* **6**(6), 631-643.
[3] Zhang B., Cullen M., Kilpatrick T. (2016) Spalling of heated high performance concrete due to thermal and hygric gradients. *Advances in Concrete Construction* **4** (1), 01-14.
[4] Firmo J.P., Correira J.R., França P. (2012), "Fire behaviour of RC beams strengthened with CFRP laminates: Protection systems with insulation of the anchorage zones". *Composites Part B:* **43,** 545-1556.
[5] Zhang H.Y., Yan J., Kodur V., Cao L. (2019), Mechanical behavior of concrete beams shear strengthened with textile reinforced geopolymer mortar, *Engineering Structures* **196**, article 109348.
[6] Awani O., El-Maaddawy T., El Refai A. (2016), Numerical simulation and experimental testing of concrete beams strengthened in shear with fabric-reinforced cementitious matrix, *Journal of Composites for Construction***, 20** (6).
[7] Tetta Z.C., Bournas D.A. (2016), "TRM vs FRP jacketing in shear strengthening of concrete members subjected to high temperatures". *Composites Part B: Engineering* **106**, 190-205.
[8] Tetta Z.C., Koutas L.N., Bournas D.A. (2015), ''Textile-reinforced mortar (TRM) versus fiber-reinforced polymers (FRP) in shear strengthening of concrete beams'', Composites Part B **77**, 338-348
[9] Verbruggen S., Tysmans T., Wastiels J. (2014), TRC or CFRP strengthening for reinforced concrete beams: An experimental study of the cracking behavior, *Engineering Structures* **77**, 49-56.
[10] Contamine R., Junes A., Si Larbi A (2014), "Tensile and in-plane shear behaviour of textile reinforced concrete: Analysis of a new multiscale reinforcement", *Construction and Building Materials* **51**, 405-413.
[11] Elsanadedy H.M., Almusallam T.H., Alsayed S.H., Al-Salloum Y.A. (2013) Flexural strengthening of RC beams using textile-reinforced mortar – Experimental and numerical study, Compos. Structures **97**, 40-55
[12] Contamine R., Si Larbi A., Hamelin P. (2013), "Identifying the contributing mechanisms of textile reinforced concrete (TRC) in the case of shear repairing damaged and reinforced concrete beams", *Engineering Structures*, **46**, 447-458
[13] Al-Salloum1 Y.A., Elsanadedy H.M.; Alsayed S.H.; Iqbal R.A. (2012) Experimental and numerical study for the shear strengthening of reinforced concrete beams using textile-reinforced mortar, J. Compos. Constr., **16**(1): 74-90.
[14] Si Larbi A., Contamine R., Hamelin P. (2012), "TRC and hybrid solutions for repairing and/or strengthening reinforced concrete beams", *Engineering Structures,* **45**, 12-20.
[15] Contamine R., Si Larbi A., Hamelin P. (2011), "Contribution to direct tensile testing of textile reinforced concrete (TRC) composites". *Materials Science and Engineering A*; **29528,** 8589– 8598.
[16] Tlaiji T., Vu X.H., Ferrier E., Si Larbi A. (2018), "Thermomechanical behaviour and residual properties of textile reinforced concrete (TRC) subjected to elevated and high temperature loading: experimental and comparative study". *Composites Part B* **144**, 99–110.
[17] Truong B. T., Si Larbi A., Limam A. (2016) « Numerical modelling of reinforced concrete beams repaired by TRC composites ». Composite Structures 152 779-790.
[18] Nguyen T.H., Vu X.H., Si Larbi A., Ferrier E. (2016), "Experimental study of the effect of simultaneous mechanical and high-temperature loadings on the behaviour of textile-reinforced concrete (TRC)". *Construction and Building Materials* **125**, 253-270.
[19] Ehlig D., Hothan S. (2011), "Reinforced concrete slabs strengthened with textile reinforced concre te sujected to fire", *2nd International RILEM Workshop on Concrete Spalling due to Fire Exposure*, 5-7 Octorber 2011, Delft, The Netherlands.
[20] Bisby L. (2016), "Fire resistance of textile fiber composites used in civil engineering", *Textile Fibre Composites in Civil Engineering*, 169-185.
[21] Bisby L. (2013), Stratford T., Hart C., Farren S., "Fire performance of well-anchored TRM, FRCM and FRP flexural strengthening systems", *Advanced Composites in Construction*, Network Group for Composites in Construction.

[22] Michels J., Zwicky D., Scherer J., Harmanci Y.E., Motavalli M. (2014), "Structural strengthening of concrete with fiber reinforced cementitious matrix (FRCM) at ambient and elevated Temperature - Recent Investigations in Switzerland". *Advances in Structural Engineering*, **17** (12), 1785-1799.
[23] Maroudas S.R., Papanicolaou C.C.G. (2017), "Effect of high temperatures on the TRM-to-masonry bond", *Key Engineering Materials* **747**, 533-541.
[24] Raoof S.M., Bournas D.A (2017a), "TRM versus FRP in flexural strengthening of RC beams: Behaviour at high temperatures", *Construction and Building Materials* **154**, 424-437.
[25] Kapsalis P., El Kadi M., Vervloet J., De Munck M., Wastiels J., Triantafillou T., Tysmans T. (2019), Thermomechanical behavior of textile reinforced cementitious composites subjected to fire, Applied Sciences (MDPI), **9**, 747.
[26] Buttner T., Orlowsky J., Raupach M. (2014), "Fire resistance tests of textile reinforced concrete under static loading - results and future developments", *Proceedings of the Fifth International RILEM Workshop on High Performance Fiber Reinforced Cement Composites* (HPFRCC5), 2014.
[27] Rambo D.A.S., Silva F.d.A., Filho R.D.T., Ukrainczyk N., Koenders E. (2016), "Tensile strength of a calcium-aluminate cementitious composite reinforced with basalt textile in a high-temperature environment", *Cement & Concrete Composites* **115**, 183-193.
[28] Donnini J., Basalo F.D.C., Corinaldesi V., Lancioni G., Nanni A. (2017), "Fabric-reinforced cementitious matrix behaviour at high-temperature: experimental and numerical results", *Composites Part B*, **108**: 108-121.
[29] Drach B., Drach A., Tsukrov I., 2014. Finite element models of 3D woven composites based on numerically generated micro-geometry of reinforcement.
[30] Firmo J.P., Arruda M.R.T., Correia J.R., Rosa I.C. (2018), "Three-dimensional finite element modelling of the fire behaviour of insulated RC beams strengthened with EBR and NSM CFRP strips", *Composite Structures* **183**, 124–36.
[31] Firmo J.P., Arruda M.R.T., Correia J.R. (2014), "Contribution to the understanding of the mechanical behaviour of CFRP-strengthened RC beams subjected to fire: Experimental and numerical assessment". *Compos Part B Eng.*; **66**, 15–24.
[32] Hawileh R.A., Naser M., Rasheed H.A. (2011) Thermal-stress finite element analysis of CFRP strengthened concrete beam exposed to top surface fire loading, *Mechanics of Advanced Materials and Structures*, **18** (3), 172-180.
[33] Hawileh R.A.; Naser M.; Zaidan W.; Rasheed H. A. (2009), "Modeling of insulated CFRP-strengthened reinforced concrete T-beam exposed to fire". *Eng. Struct.* **31** (12), 3072–3079.
[34] Nigro E., Cefarelli G., Bilotta A., Manfredi G., Cosenza E. (2011) "Fire resistance of concrete slabs reinforced with FRP bars, part II: experimental results and numerical simulations on the thermal field". *Compos. Part B Eng.* **42** (6), 1751–1763.
[35] Adelzadeh M., Hajiloo H., Green M.F. (2014), "Numerical Study of FRP Reinforced Concrete Slabs at Elevated Temperature". *Polymers*, **6**:408–22.
[36] Naser M. Z., Hawileh R. A., Abdalla J. A. (2019), "Fiber-reinforced polymer composites in strengthening reinforced concrete structures: A critical review". *Engineering Structures 198 109542.*
[37] Dwaikat M. B., Kodur V. K. R. (2009) "Response of restrained concrete beams under fire exposure", *Journal of structural engineering ASCE. Vol. 135, issue 11.*
[38] Kodur V., Dwaikat M., Raut N., (2009), « Macroscopic FE model for tracking the fire response of reinforced concrete structures ». *Engineering Structures 31 2368-2379*
[39] Carlo T.B., Rodrigues J.P.C., De Lima R.C.A, De Lima R.C.A (2018) Experimental analysis on flexural behaviour of RC beams strengthened with CFRP laminates and under fire conditions, *Composite Structures* 189, 51629-528.
[40] Aqeel A., Venkatesh K. (2011), "The experimental behavior of FRP-strengthened RC beams subjected to design fire exposure", Engineering Structures 33 2201-2211.
[41] MSC Marc volume A (2014) MSC MARC MENTAT software, Volume A: theory and user information.
[42] Bary B., Marcus V.G. d.M., Poyet S., Durand S. (2012) «Simulation of the thermo-hydro-mechanical behaviour of an annular reinforced concrete structure heated up to 200 °C». *Engineering structures* **36**, 302-315.
[43] Eurocode 3, EN 1993-1-2 (1993), *Eurocode 3: Design of steel structures*- Part 1-2: General rules- Structural fire design.
[44] Eurocode 2, EN 1992-1-2 (1992), *Eurocode 2, design of concrete structures,* Part 1.2: General rules – structural fire design. Brussels: Commission of the European Communities; 2004.
[45] Douk N., Si Larbi A., Vu X.H, Audebert M. (2018). "State of the art of the simple thermal approach for concrete and numerical contribution to the sensitivity of concrete temperature fields on its thermal behaviour at high temperatures", *Academic Journal of Civil Engineering*, **36**(1), 340-343.
[46] Nguyen V.T. (2013). « Comportement des bétons ordinaire et à hautes performances soumis à haute température : application à des éprouvettes de grandes dimensions » (in French), Thesis dissertation, University of Cergy Pontoise, France.
[47] Liao F., Huang Z. (2015), "An extended finite element model for modelling localized fracture of reinforced concrete beams in fire". *Computers and structures* **152,** 11-26.
[48] Takahashi Y. (1983). Elastic-plastic constitutive modeling of concrete. *LMFBR—Structural Materials and Design Engineering: Base Technology, United States, 1983.*
[49] Bazant Z.P., Kaplan M.F. (1996). Concrete at high temperatures : material properties and mathematical models, *Civil and Environmental Engineering*, Addthermon-Wesley.
[50] Tlaiji T., Vu X.H., Ferrier E. (2017a) "RC-M100 composite behaviour laws as a function of temperature" (scientific report written in French). Research report number 10 of the UCBL/LMC2 for the project PRORETEX II. April 2017.
[51] Colombo I., Colombo M., Magri1 M., Zani1 G. and di Prisco1 M (2011). "Textile Reinforced Mortar at high temperature". *Applied Mechanics and Materials. July2011.*
[52] Buyukuzturk O. (1975), "Nonlinear analysis of reinforced concrete structures". *Comput. Struct.* 7, 149–155.
[53] Kupfer H., Hilsdorf H.K., Rusch, H., 1969. "Behavior of concrete under biaxial stresses" **66**, 656–666.
[54] Ohnami M., Sakane M., Nishimo S. (1988), "Cyclic behavior of a type 304 Stainless steel in biaxial stress states at elevated temperatures", *International Journal of Plasticity*, **4**, 77-89.
[55] Rossi P. (2011). "Damage mechanisms analysis of a multi-scale piber reinforced cement-based composite subjected to impact loading conditions. *Presented at the 2nd International RILEM Coference on Strain Hardening Cementitious Composites" 12-14 December 2011*, Rio de Janeiro, Brazil, pp. 37–44.
[56] Peled A. (2011). "Strain hardening behavior of textile reinforced concrete (TRC)". Presented at the 2nd *International RILEM Conference on Strain Hardening Cementitious Composites* 12-14 December 2011, Rio de Janeiro, Brazil, pp. 45–52.
[57] Si Larbi A, Agbossou A, Hamelin A., (2013) « Experimental and numerical investigations about textile-reinforced concrete and hybrid solutions for repairing and/or strengthening reinfroced concrete beams ». *Composite Structures 99 152-162.*

[58] Giorgio C. I., Colombo M., di Prisco M., Pouyaei F., (2018) « Analytical and numerical prediction of the bending behaviour of textile reinfroced concrete sandwich beams ». *Journal of Building Engineering 17 183-195.*

[59] Vervloet J., Tysmans T., El Kadi M., De Munck M., Kapsalis P., Itterbeeck P. V., Wastiels J., Hemelrijck D. V. (2019). « Validation of a numerical bending model for sandwish beams with Textile-Reinforced cement faces by means of digital image correlation ». *Mechanics of Materials and Constructions 1253.*

[60] Tlaiji Tala (2018) "Développement et caractérisation du comportement thermomécanique des matériaux composites TRC". Thesis at the university of Lyon 1 Claude Bernard (in French).

[61] Tran N.C., (2011) "Développement d'un modèle d'interface acier-béton à haute température: modélisation des structures en béton exposées au feu". Thesis at Paris-EST university Ecole des ponts Paristech.

[62] Raouffard M. M., Nishiyama M. (2016) « Fire resistance and residual strength of RC frame" Department of Architecture and Architectural Engineering Kyoto University.

[63] NF EN 1363-1 (2020), Essais de résistance au feu - Partie 1 : exigences générales - Essais de résistance au feu - Partie 1 : Exigences générales (in French).

[64] Kodur V.K., Agrawal A. (2015) «Critical Factors Governing the Residual response of Reinforced Concrete Beams Exposed to Fire", Fire Technology volume 52, pages967–993(2016).